

Hydrogen bonding in lithium hydrazinium sulfate
by Francis Luther Howell

A thesis submitted to the Graduate Faculty in partial fulfillment of the requirements for the degree of DOCTOR OF PHILOSOPHY in Physics
Montana State University
© Copyright by Francis Luther Howell (1969)

Abstract:
The nuclear magnetic resonance spectrum of deuterons in LiN2D5SO4 has been studied in detail between 78 and 458°K. The spectrum at 78° is related to the deuterons of a static N2D5^+ i o n . The electric quadrupole coupling constants, the asymmetry parameters, and the orientations of electric field gradient (efg) tensors relative to the crystal axes were obtained at 78, 193, 298, 338, 368 and 438%deg;K. Above 110°K the lines due to the deuterons of the ND3 group broaden and merge to a single pair of lines which is still evident at 195°C. The lines corresponding to the deuterons of the ND2 group merge to a single pair between O° and 50°C. These line mergers are related to the motion of the ND3 and ND2 groups and estimates of the activation energy and jump times of these motions are made. Because of the symmetry of the crystal the absence of line doubling indicates that ferroelectric domain reversal may be due to reflection of the structure through the ab plane.

Measurements of the electrical conductivity and the ac dielectric constant were made on both deuterated and undeuterated samples. The c axis ac dielectric constant was found to be quite large. Estimates of the activation energy and correlation time for the dielectric relaxation were made.

The spin-lattice relaxation times for the merged ND3 and ND2 lines were measured over the temperature range from 155°K to 422°K. The results are found to be in good agreement with the assumption that the relaxation is due to fluctuations in the electric quadrupole coupling energy due to ND3 and ND2 hindered rotations. In addition, evidence is found to indicate that jumping between ND2 and ND3 groups becomes important at temperatures above 75°C. None of the measurements discussed indicate that the crystal undergoes a ferroelectric transition below 200°C.

HYDROGEN BONDING IN LITHIUM HYDRAZINIUM SULFATE

by

FRANCIS LUTHER HOWELL

A thesis submitted to the Graduate Faculty in partial fulfillment of the requirements for the degree

of

DOCTOR OF PHILOSOPHY

in

Physics

Approved:

Nathaniel J. Hutzman
Acting Head, Major Department

V. Hugo Schmidt
Chairman, Examining Committee

R. Goering
Graduate Dean

MONTANA STATE UNIVERSITY
Bozeman, Montana

December, 1969

ACKNOWLEDGEMENTS

The author wishes to thank the National Institutes of Health and the National Science Foundation for financial assistance and for providing funds for the apparatus used in this research. He extends particular thanks to his advisor, Dr. V. Hugo Schmidt, for helpful discussion, guidance and encouragement always forthcoming when needed. To R.R. Knispel he is grateful for stimulating discussion, for the loan of apparatus and computer programs and for help with the experiment. He thanks Robert Parker for the loan of apparatus and for his help in using the NMR pulse apparatus. To Fred Blankenburg he extends thanks for generous assistance with the electronics apparatus used. Thanks is extended to P. LaPere for help with the drawings. To Drs. W. C. Hamilton and F. Ross thanks is extended for their kindness in supplying the author with information on the structure of deuterated lithium hydrazinium sulfate prior to publication. The author offers his deepest thanks to his wife, Marion, and to his children Shap, Dan, and Alice, for their constant help and confidence which made the completion of this program possible.

TABLE OF CONTENTS

Chapter		Page
	LIST OF TABLES	v
	LIST OF FIGURES	vi
	ABSTRACT	ix
I	INTRODUCTION	1
II	DEUTERON ELECTRIC FIELD GRADIENT TENSORS AT 77°K	6
	Structure	6
	NMR Spectrum	11
	Discussion	16
III	DEUTERON MOTION	28
	Conductivity and Dielectric Constant	28
	Previous NMR Studies	36
	High Temperature Spectrum	41
	Exchange Probability	50
	Discussion	71
IV	EXPERIMENTAL	74
	Crystal Preparation	74
	NMR Spectra	74
	Conductivity and Dielectric Constant	79
	Relaxation Time	86
	APPENDIX	91
	Appendix A	91
	Appendix B	98
	Appendix C	108
	LITERATURE CITED	111

LIST OF TABLES

Table		Page
I	Coordinates of the Constituents of the Unit Cell of LiHzS	7
II	Coupling Constants, Asymmetry Parameters and Orientation of Principal Axes of efg Tensors at 78^{o} and 193^{o}K	20
III	N-H...X Bond Lengths and Bond Angles	24
IV	Coupling Constants and Asymmetry Parameters for N-D Bonds of Several Compounds	25
V	Conductivities and Conductivity Activation Energies	29
VI	Coupling Constants, Asymmetry Parameters and Orientation of Principal Axes of efg Tensors above 273^{o}K	47
VII	Efg Components in Crystal System	62
VIII	Efg Components in Rotated System, z' $\|\|$ a . .	63
IX	Efg Components in Rotated System, z' 18^{o} from z' $\|\|$ a	64
X	Calculated Values for the Transition Probabilities P_1 and P_2	66
XI	Inter-site Distances for $N_2D_5SO_4$ (After Ross and Hamilton(40)).	109

LIST OF FIGURES

Figure		Page
1	Structure of Lithium Hydrazinium Sulfate Viewed Down the c Axis	9
2	Detail of N-H...N Bonding	9
3	Sketch of the Hydrazinium Ions Showing the ND_3 and ND_2 Grouping	10
4	Typical NMR Spectra of the Deuterons at Liquid Air Temperature	14
5	Quadrupole Splitting of Deuterons vs Rotation Angle About the a Crystallographic Axis at Liquid Air Temperature	17
6	Quadrupole Splitting of Deuterons vs Rotation Angle About the b Crystallographic Axis at Liquid Air Temperature	18
7	Quadrupole Splitting of Deuterons vs Rotation Angle About the c Crystallographic Axis at Liquid Air Temperature	19
8	Plot of Coupling Constant as a Function of the Square of the X-H Stretching Frequency	26
9	Log of Electrical Conductivity vs Temperature .	31
10	Log of Real and Imaginary Parts of the ac Dielectric Constant vs Frequency	32
11	Plot of the Imaginary vs the Real Part of the ac Dielectric Constant	34
12	Log of Real and Imaginary Parts of the ac Dielectric Constant vs Temperature	35
13	Proton Second Moment vs Temperature (After Cuthbert and Petch[11])	37
14	Proton Second Moment vs Temperature (After McClement, Pintar and Petch[12])	39

Figure		Page
15	Proton Spin Lattice Relaxation Time vs Temperature (After McClement, Pintar and Petch(12))	40
16	NMR Spectrum of Deuterons at Selected Temperatures	42
17	Quadrupole Splitting of Deuterons vs Rotation Angle About the a Crystallographic Axis at 95°C	43
18	Quadrupole Splitting of Deuterons vs Rotation Angle About the b Crystallographic Axis at 95°C	44
19	Quadrupole Splitting of Deuterons vs Rotation Angle About the c Crystallographic Axis at 95°C	45
20	Sketch of Line Separation and Broadening . . .	52
21	Log Jump Probability vs Temperature for ND_2 .	56
22	Log Jump Probability vs Temperature for ND_3 . .	57
23	Deuteron Spin Relaxation Time vs Reciprocal Temperature	60
24	Block Diagram of NMR Experiment	77
25	Block Diagram of Conductivity Experiment . . .	80
26	Equivalent Circuit of Crystal Conductivity . .	81
27	Circuit Diagram of ac Dielectric Constant Experiment	84
28	Drawing of ac Dielectric Constant Sample Probe	85
29	Block Diagram of Pulsed NMR Apparatus	88
30	Zeeman Levels of I = 1 System with Quadrupole Perturbation	95
31	Populations of Nuclear Levels for Symmetric Saturation	104
32	Populations of Nuclear Levels for Saturation of $\Delta m = 0 \leftrightarrow -1$ Transition	104

Figure		Page
33	Populations of Nuclear Levels for Jumping Between ND_2 and ND_3 System	106
34	Stereoscopic Illustration of Structure	110

ABSTRACT

The nuclear magnetic resonance spectrum of deuterons in $LiN_2D_5SO_4$ has been studied in detail between 78 and 458°K. The spectrum at 78° is related to the deuterons of a static $N_2D_5^+$ ion. The electric quadrupole coupling constants, the asymmetry parameters, and the orientations of electric field gradient (efg) tensors relative to the crystal axes were obtained at 78, 193, 298, 338, 368 and 438°K. Above 110°K the lines due to the deuterons of the ND_3 group broaden and merge to a single pair of lines which is still evident at 195°C. The lines corresponding to the deuterons of the ND_2 group merge to a single pair between 0° and 50°C. These line mergers are related to the motion of the ND_3 and ND_2 groups and estimates of the activation energy and jump times of these motions are made. Because of the symmetry of the crystal the absence of line doubling indicates that ferroelectric domain reversal may be due to reflection of the structure through the ab plane.

Measurements of the electrical conductivity and the ac dielectric constant were made on both deuterated and undeuterated samples. The c axis ac dielectric constant was found to be quite large. Estimates of the activation energy and correlation time for the dielectric relaxation were made.

The spin-lattice relaxation times for the merged ND_3 and ND_2 lines were measured over the temperature range from 155°K to 422°K. The results are found to be in good agreement with the assumption that the relaxation is due to fluctuations in the electric quadrupole coupling energy due to ND_3 and ND_2 hindered rotations. In addition, evidence is found to indicate that jumping between ND_2 and ND_3 groups becomes important at temperatures above 75°C. None of the measurements discussed indicate that the crystal undergoes a ferroelectric transition below 200°C.

CHAPTER I INTRODUCTION

An explanation of the ferroelectric behavior of certain hydrogen bonded crystals* derives from understanding the environment and motion within the crystal of the protons forming the hydrogen bonds. X-ray and neutron diffraction studies are commonly used to locate the positions of atoms in the unit cell of the crystal, and may be used to obtain information on the motion of the atoms. Conductivity and dielectric constant measurements also yield information about the motion of the constituents of the crystal.

However, the usefulness of neutron studies to obtain information on motion is limited in the following respect. Since exchange between sites, such as hindered rotation of a group, probably takes place in such a fashion that the time spent "jumping" between sites is a very small part of the total time, the neutron diffraction results will reflect the stationary location of the group. Because of this, neutron diffraction studies give good indication of vibrational or torsional motions, for which time spent out of the equilibrium site is large, but little information

---

*Discussion of hydrogen bonded ferroelectrics may be found in reference 1. For a detailed discussion of KH_2PO_4, a representative of this class which has been studied in detail, see references 2, 3, 4, 5, 6, and 7.

about motions such as are of primary interest in this work.

Conductivity studies of hydrogen bonded crystals are difficult. The conductivities commonly encountered are small, $\sim 10^{-8}/\Omega$ cm or less, and impurities and crystal defects can introduce relatively large errors. At best, measurements of conductivity and dielectric constant deal with bulk properties of the crystal, making it difficult to distinguish the various atomic effects unambiguously.

An experiment which has proven particularly useful in obtaining information about the environment and motion of nuclei is the observation of the nuclear magnetic resonance (NMR) spectrum.*

The nucleus of primary interest is the proton. The NMR spectrum of the proton in solids is generally a single wide line, and proton wide-line NMR studies are limited to measurement of line width and of the spin-lattice relaxation time. From such studies much can be inferred about motion of the protons and their relative location in the crystal. However, no measure of the local electrical environment is possible with the proton since it has no electric moments. Because of their approximate chemical equivalence it is possible to substitute deuterons for

---

*Discussion of this type of experiment is included in references 8 and 9.

protons. This can be done by crystallizing from a heavy water solution in the case of most water soluble compounds. The deuteron has an electric quadrupole moment and interacts with the electric field gradient (efg) at its location. This interaction modifies its NMR spectrum in such a fashion that the determination of the efg tensor at the deuteron site is made possible.

Lithium hydrazinium sulfate (LiHzS) is a ferroelectric crystal,[10] and neutron diffraction studies[11] of the structure have established that the protons of the hydrazine group are all involved in hydrogen bonds. Nuclear magnetic resonance studies of the protons and Li^7 nuclei in LiHzS have been carried out.[12,13] Based on these studies, jumping of the protons between bond sites and other motions have been hypothesized.

Although the studies mentioned above answer many questions about the structure and indicate that the protons undergo certain motions, several important questions remain unanswered. Specifically, what are the motions of the protons? Is there a ferroelectric transition below the decomposition temperature of the crystal? What, if any, structural changes occur in the crystal as it is heated? Is there any change in the ordering of the protons when the crystal changes polarization? This work deals with the attempt to answer these questions by a study of the nuclear

magnetic resonance spectrum of deuterons in the deuterated crystal, $LiN_2D_5SO_4$, and by measurements of the electrical conductivity and ac dielectric constant of the normal and deuterated crystals.

The spectrum of the deuterons was studied below the temperature at which jumping among sites becomes important, and the results are discussed in Chapter II. The NMR spectrum at higher temperature reflects inter-site exchange and the third chapter is devoted to the measurements which reveal this motion. A complete study of the NMR spectrum of the deuterons was carried out to above 150°C. In addition, the deuteron line width was measured as a function of temperature through the critical temperature regions. On the basis of these measurements a calculation of the exchange probability for the motion causing the line width change was done. It was hoped that the electric field gradient measured at elevated temperatures would reflect the structural change suggested by Cuthbert and Petch[12] as a result of their observation of a change in the Li^7 NMR spectrum with temperature.

The dielectric behavior was studied because the nature of the dielectric anomaly at a phase transition indicates what type of ferroelectric transition occurs.

Finally the spin-lattice relaxation time was measured

for deuterons of the groups which undergo motion. Using the efg data discussed in Chapter III, the relaxation mechanism was related to the fluctuations in the efg due to exchange between sites. The activation energies for the motions obtained by the different measurements were compared.

Relatively few studies have been carried out to determine the values of the efg tensors at the sites of deuterons in N-D...N or N-D...O bonds. Because of the numerous analogies to these bonds found in compounds of biological significance, it would seem that simply the accumulation of information about the efg tensors and the activation energies for motion between bonds of this type is worth while. Summarized in a table in Chapter II is pertinent information on some of the nitrogen compounds which have been studied.

CHAPTER II

DEUTERON ELECTRIC FIELD GRADIENT TENSORS AT 77°K

STRUCTURE.

The structure of lithium hydrazinium sulfate ($LiN_2H_5SO_4$) has been studied by means of x-ray[14,15,16] and neutron[11] diffraction. Table I compares the coordinates of the constituents of LiHzS found by these experiments.

LiHzS is orthorhombic of space group $Pbn2_1$,[15] with four molecular units per unit cell. Padmanabhan and Balasubramanian[11] (hereafter denoted by PB) report cell dimensions a=9.93, b=8.969, and c=5.178 Å. Brown[15] has found for the cell dimensions a=8.99, b=9.94, and c=5.18 Å.*

The lithium and sulfur atoms are located at the centers of tetrahedra of oxygen atoms. As is indicated in Fig. 1, these tetrahedra have common apices and form a lattice-work with channels running parallel to the c axis. These channels contain the hydrazinium ions which are hydrogen bonded to atoms in the surrounding lattice and to nitrogen atoms adjacent in the c direction. The

---

*The exchange in the assignment of the a and b crystal axes by PB will not be followed in this thesis, rather the assignment made by Brown will be observed.

TABLE I

Atomic Parameters Obtained by X-ray and Neutron Studies
Standard Deviation Is That Quoted by P & B for Their Data

		Brown[15]	Van den Hende & Boutin[16]	Padmanabhan & Balasubramanian[11]	Standard Deviation[11]
S	x	0.1286	0.1290	0.126	0.001
	y	0.1579	0.1589	0.159	0.001
	z	0.250	0.250	0.250	0.002
O(1)	x	0.106	0.1068	0.106	0.002
	y	0.191	0.1870	0.193	0.001
	z	0.519	0.5434	0.533	0.002
O(2)	x	0.154	0.1511	0.153	0.002
	y	0.010	0.0132	0.012	0.001
	z	0.220	0.2296	0.229	0.001
O(3)	x	0.259	0.2558	0.259	0.001
	y	0.230	0.2335	0.230	0.001
	z	0.149	0.1626	0.151	0.002
O(4)	x	0.497	0.4904	0.498	0.001
	y	0.302	0.3048	0.304	0.001
	z	0.596	0.6016	0.600	0.002
N(1)	x	0.418	0.4193	0.414	0.001
	y	0.002	0.0285	0.024	0.001
	z	0.746	0.7405	0.743	0.002
N(2)	x	0.217	0.2137	0.213	0.001
	y	0.440	0.4460	0.440	0.001
	z	0.742	0.7346	0.739	0.002
Li	x	0.437	0.433	0.422	0.003
	y	0.332	0.339	0.336	0.003
	z	0.253	0.271	0.256	0.003
H(1)	x	____	____	0.381	0.004
	y	____	____	0.118	0.003
	z	____	____	0.796	0.003

TABLE I (continued)

		Brown[15]	Van den Hende & Boutin[16]	Padmanabhan & Balasubramanian[11]	Standard Deviation[11]
H(2)	x	____	____	0.467	0.004
	y	____	____	0.036	0.004
	z	____	____	0.571	0.004
H(3)	x	____	____	0.189	0.003
	y	____	____	0.345	0.003
	z	____	____	0.677	0.003
H(4)	x	____	____	0.247	0.005
	y	____	____	0.428	0.004
	z	____	____	0.924	0.004
H(5)	x	____	____	0.292	0.004
	y	____	____	0.469	0.002
	z	____	____	0.601	0.003

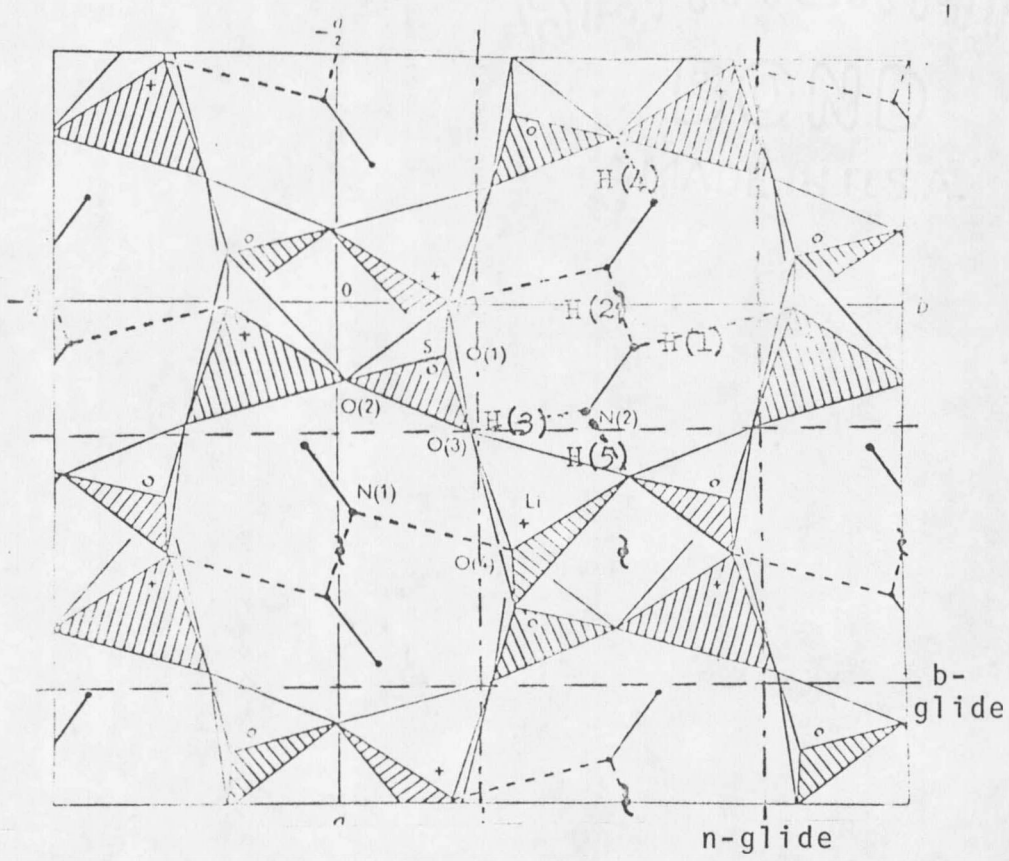


Fig. 1 A View of LiHzS Projected Down the c Axis. (After Brown(15))

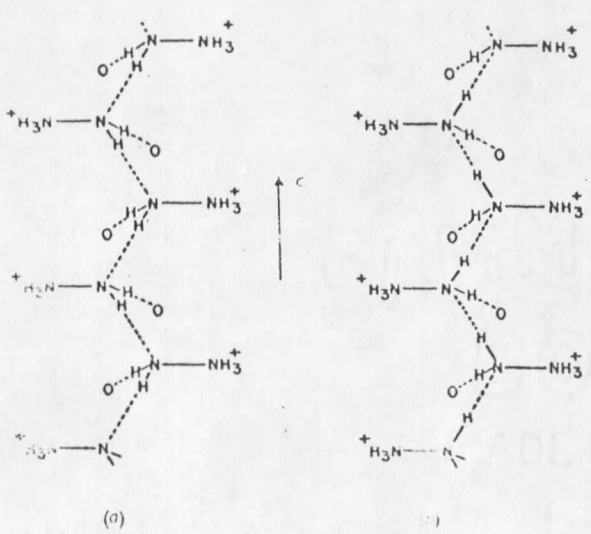


Fig. 2 Two Alternate Arrangements Possible for N-H...N-H... Chain if the Hydrogen Bonds Are Ordered. (After Brown(15))

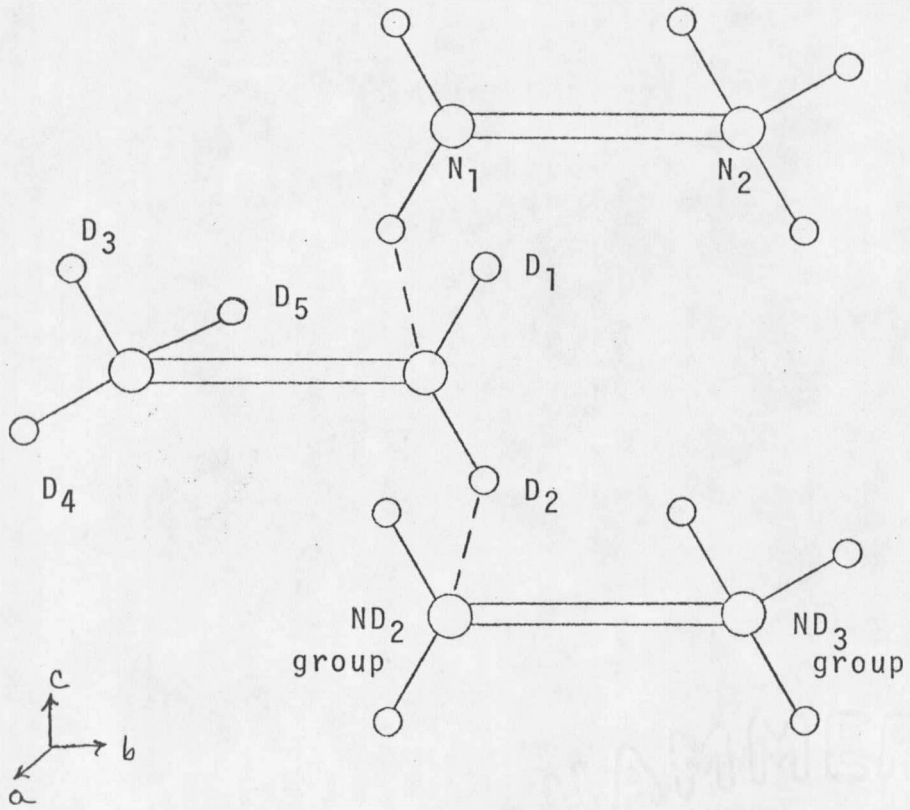


Fig. 3. Sketch Showing the General Arrangement of the ND_3 and ND_2 Groups and the Bonding Between Hydrazine Groups.

proton in a hydrogen bond is found at a position between the two atoms with which it forms the bond. In general the proton is nearer to one of the bonded atoms than the other. The bonded atom which is closest to the proton is denoted the donor, and the further bonded atom is called the acceptor. In LiHzS, the donor to proton distances are about 1 Å, and the acceptor to proton distances are roughly 2 Å. The nitrogen is the donor in each N-H...O bond. The nitrogen at the NH_3 end of the N_2H_5 group takes part in three N-H...O bonds. The nitrogen at the NH_2 end is bonded to one oxygen and two other nitrogens. These latter bonds form N-H...N-H... chains along the c direction of the crystal. Following the notation of PB, the proton sites in these bonds are referred to as site 2 whereas the other proton site at the NH_2 end of the N_2H_5 group is in a N-H...O bond and is denoted as site 1. The labeling of sites 3, 4 and 5 is indicated in Fig. 1. From their neutron diffraction study, PB have concluded that most or all of the site 2 protons are ordered in the arrangement pictured in Fig. 2a as opposed to the arrangement in Fig. 2b. They further conclude that no hindered rotation of NH_3 or NH_2 groups takes place at room temperature.

NMR SPECTRUM.

The NMR spectrum of deuterons in LiHzS was studied at

temperatures from 78°K to 463°K. The spectrum observed at 78°K does not reflect any motion within the hydrazine group and will be discussed in this chapter. The spectrum at higher temperatures reflects motion and will be discussed in Chapter III within the context of other measurements which have to do with motion of the deuterons in the crystal.

In first order the interaction between the nuclear quadrupole moment of the deuteron and the electric field gradient (efg) at the site of the deuteron splits the deuteron NMR line into two lines spaced equally above and below the position of the unperturbed line.* Since there are twenty deuterons in a unit cell, for arbitrary orientation of the crystal relative to the applied dc magnetic field H_0, the spectrum consists of forty lines. However, there are only five sites which are chemically non-equivalent. For example, the deuteron at site 1 of any one of the four hydrazine groups of a unit cell interacts with an efg possessing the same components as each of the three other site 1 deuterons of the cell. The four site 1

---

*Appendix A contains a discussion of the nuclear quadrupole interaction and the technique of nuclear magnetic resonance spectroscopy employed in the determination of the efg tensor carried out in this study.

deuterons differ only in the direction of the axes of the coordinate systems in which their respective efg tensors are diagonal. A result of this chemical equivalence and of the crystal symmetry (see Fig. 1) is that if the field H_0 is made perpendicular to one of the crystal axes, at most ten pairs of lines are observed. With H_0 parallel to a crystal axis only five pairs of lines are observed.

Spectra were obtained at $2\frac{1}{2}^{o}$ intervals about the three crystal axes. Fig. 4 displays typical spectra obtained at $77^{o}K$. The data was analyzed in the following fashion. First the position of the spectral lines relative to the center of the spectrum was measured directly from the recorder chart and expressed in gauss since the experiment was done at fixed frequency. For many crystal orientations the individual spectral lines were not all distinguishable. This is shown clearly in Fig. 4b where, of the ten pairs of lines which should be discernible, five pairs are merged with the other five. The line positions were then plotted against the orientation angle, ϕ, of the crystal relative to H_0. These plots were rough fit by using a set of sine curve overlays. By using this rough fit it was possible to exclude data points having large error. The remaining points were used in a least squares computer program to calculate the curve

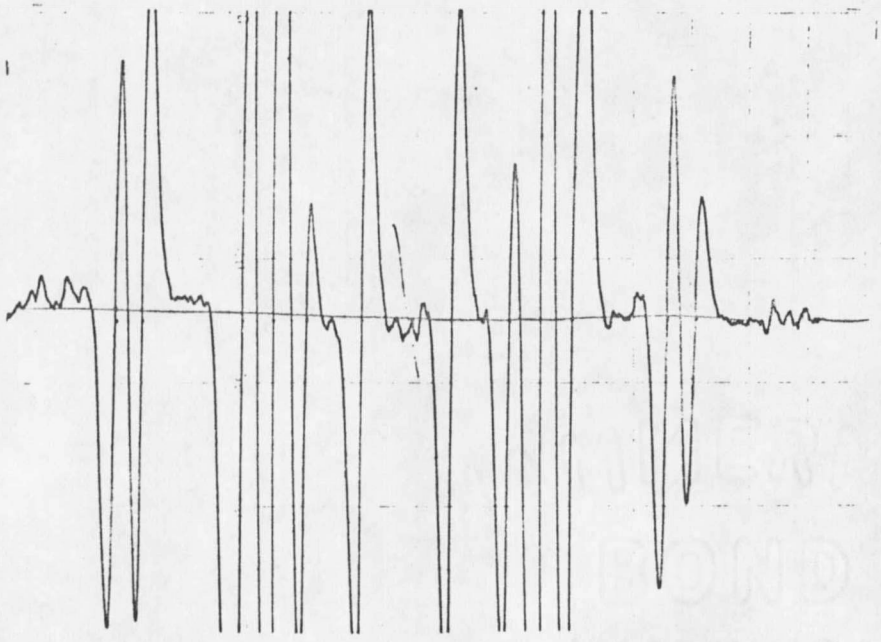


Fig. 4-a. 77°K Spectrum, Crystal Oriented 10° from a $\parallel$ to H_o with c $\perp$ to H_o.

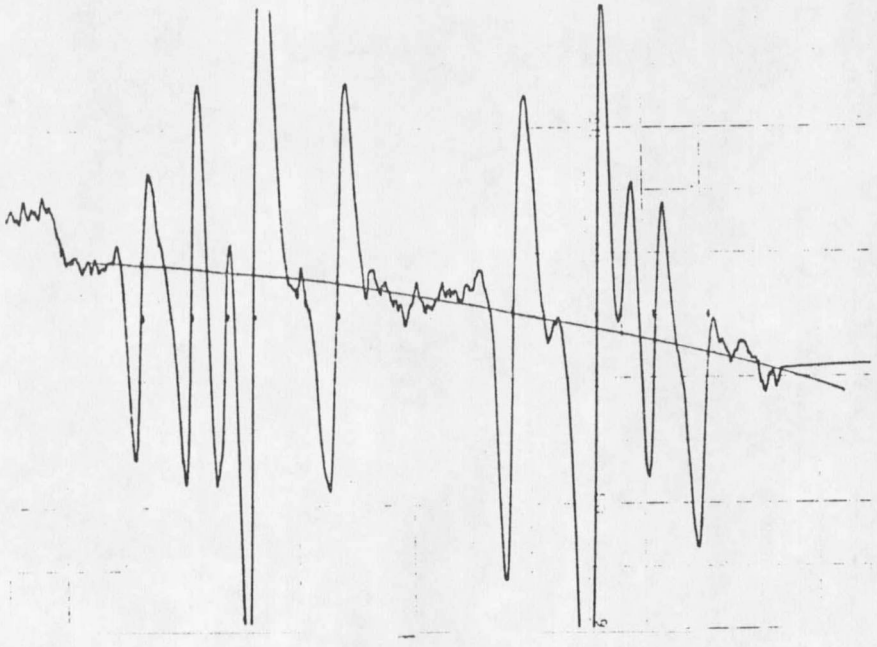


Fig. 4-b. 77°K Spectrum, Crystal Oriented 27° from a $\parallel$ to H_o with c $\perp$ to H_o.

$$2\Delta\nu = A_1 + B_1 \cos\theta + C_1 \sin\theta \qquad (2.1)$$

which best fit the data. Figs. 4, 5, and 6 are plots of the quadrupole splitting curves for the five deuteron sites for rotations about the three crystal axes.

In the case that the efg tensor is cylindrically symmetric, a rotation about an axis perpendicular to the principal axis of the efg tensor makes $2\Delta\nu$ proportional to $(1 + 3 \cos 2\theta)$ where θ measures the angle between the principal axis and the magnetic field H_0. $2\Delta\nu$ then ranges between a maximum positive value for $\theta=0$, and a maximum negative value at $\theta=90$. The negative value is just half the positive value in absolute magnitude. A rotation about an arbitrary axis includes the orientation H_0 perpendicular to the principal axis, although it does not include H_0 parallel to the principal axis. By examination of the plots of $2\Delta\nu$ (Figs. 5, 6, and 7) it can be seen that the negative maximum values are approximately the same independent of the rotation axis. This indicates the nearly cylindrical symmetry of the bonds studied. The values of the components of the efg tensor relative to the crystal axes are obtained from the A, B and C of Eq. 2.1. The efg tensor was then diagonalized and values of the coupling constant, the asymmetry parameter, and the angles

relating principal axes of the efg tensor to the crystal set were obtained. This data is given in Table II.

The estimated errors included in Table II are based on the following considerations. One source of error is misalignment of the crystal in the spectrometer head, so that the rotation axis is not quite parallel to a crystal axis. The agreement between the spectra obtained during rotations about different axes but with the same crystal axis presumably parallel to H_o was used to check the alignment. Such checks indicated that initial alignment of the crystal was accurate to better than $\frac{1}{2}^o$. The rotation angle was read directly to 1^o and estimated to 0.1^o. Error in the rotation angle is believed to be less than 0.1^o. The data points included in Figs. 5, 6 and 7 are those finally used in the least squares calculation of the curves. To test the effect of errors on the values of the efg tensor components in the principal axis system a set of varied data was fed into the diagonalization program and the estimates of error were based on the resulting variation in the output.

DISCUSSION.

The deuteron efg results are related to the LiHzS structure. (See Appendix C)

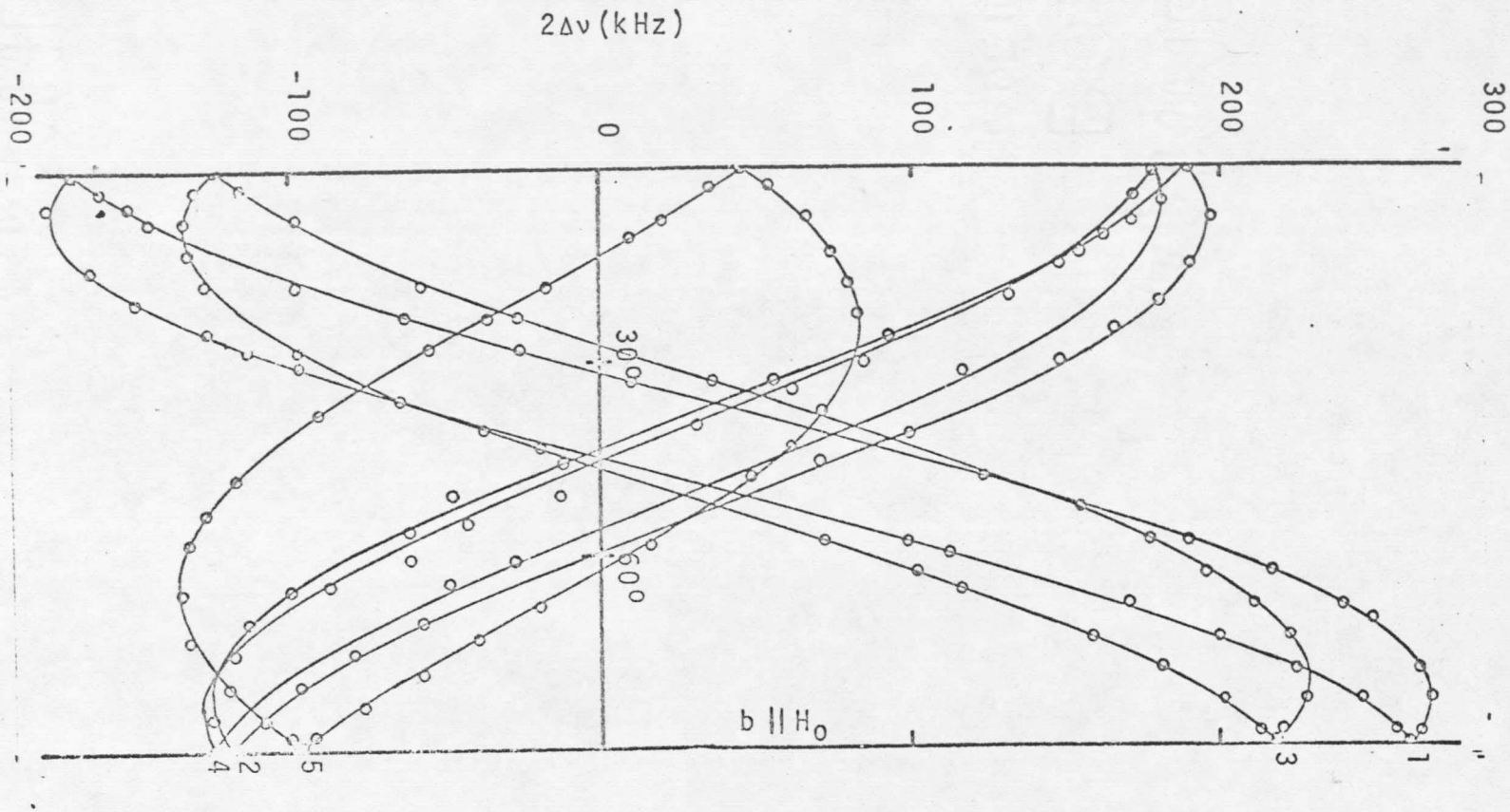


Fig. 5 Quadrupole Splitting Patterns for Rotation about the a Crystallographic Axis at Liquid Air Temperature.

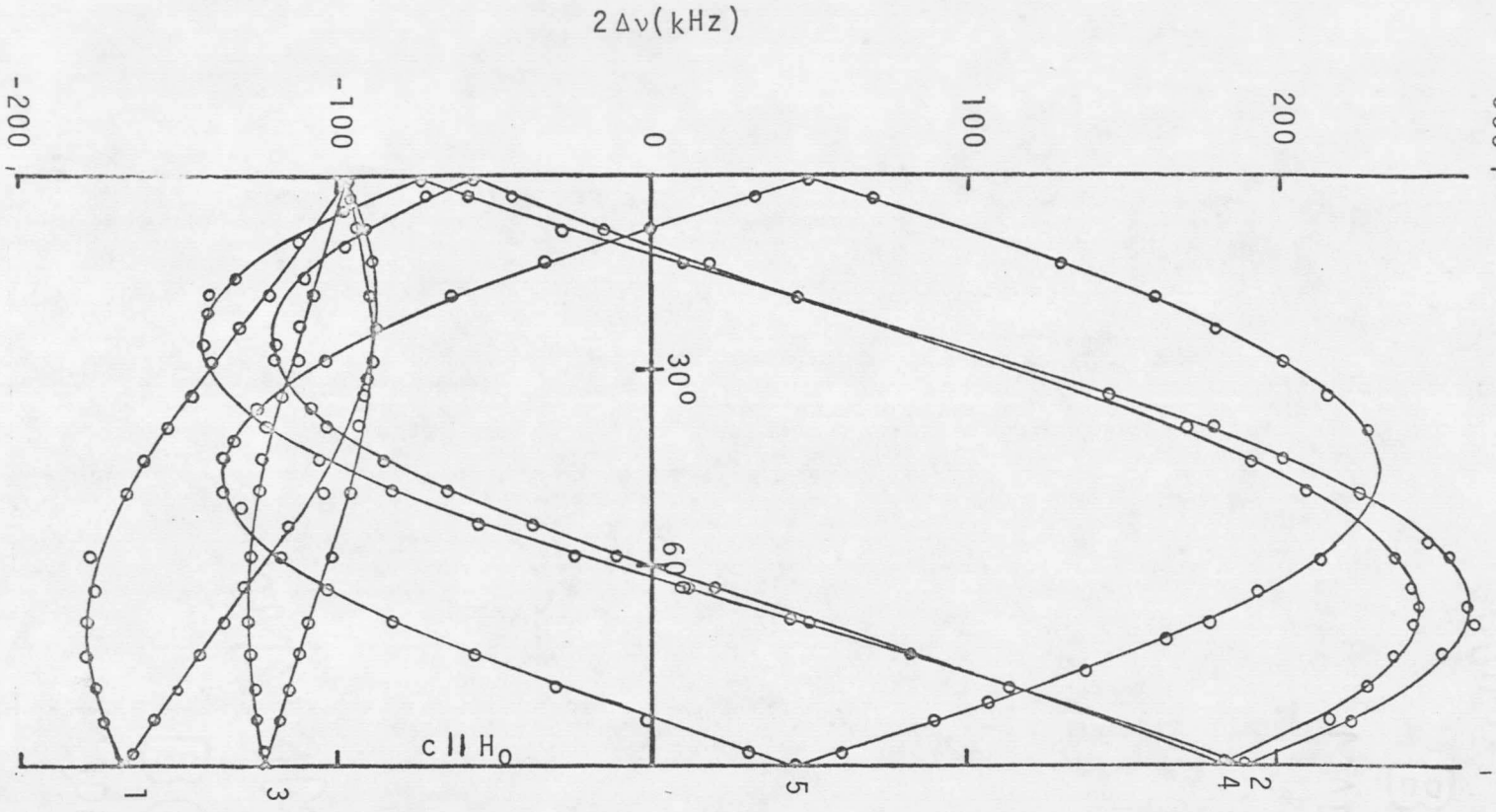


Fig. 6 Quadrupole Splitting Patterns for Rotation about the b Crystallographic Axis at Liquid Air Temperature.

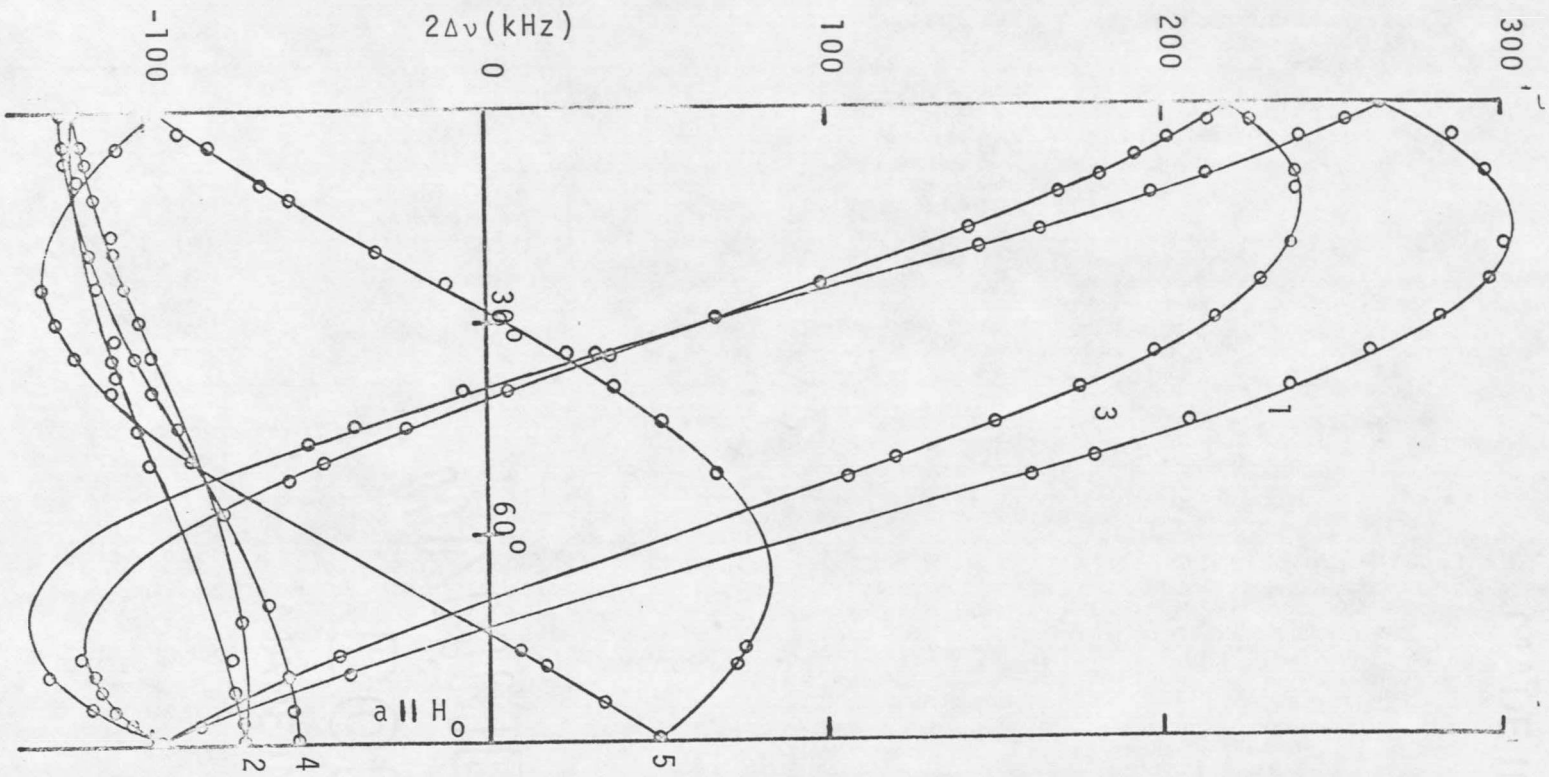


Fig. 7 Quadrupole Splitting Patterns for Rotation about the c Crystallographic Axis at Liquid Air Temperature.

TABLE II

Coupling Constant eqQ/h, Asymmetry Parameter η, and the Angle Formed Between the Principal Axis of the efg Tensor and the Crystal Axes, for the Deuteron Sites Indicated in Fig. 1. Also Listed Is the Angle Formed Between the Principal Axis of the Field Gradient and the Vector Between the Nitrogen and Proton Involved in the Bond. (All Estimated Errors for Angles Given Are $\pm 1^{o}$).

Temp. ^{o}K	Bond	eqQ/h kHz	η	θ_x	θ_y	θ_z	ϕ_{zz}, N-H angle, deg.
77	1	208±1	0.16±0.07	107	19	97	9
	2	178±1	0.12±0.07	114	6	155	4
	3	166±1	0.05±0.07	73	162	97	10
	4	167±1	0.10±0.07	114	4	25	7
	5	162±1	0.05±0.07	8	70	131	1
193	1	201±1	0.15±0.07	108	20	98	7
	2	178±1	0.08±0.07	114	5	155	4

next largest components of the efg tensor will be denoted as first principal and second principal axes respectively. As can be seen from Table II, the first principal component lies nearly along the N-H bond direction at each deuteron site. The angle so formed ranges from 1^{o} for bond 5 to about 10^{o} for bonds 1 and 3. (See Table III for bond lengths.)

If the angles formed between the efg principal axis direction and the crystal axes for one of the five sites of the unit cell are denoted θ_x, θ_y, and θ_z, then the three symmetry related sites of the cell have the corresponding angles, θ_x, $\pi-\theta_y$, θ_z; $\pi-\theta_x$, θ_y, θ_z; $\pi-\theta_x$, $\pi-\theta_y$, θ_z. This makes the efg tensor principal axis of site 1 of molecule 1 and site 3 of molecule 4 almost parallel and site 2 of molecule 1 and site 4 of molecule 4 nearly parallel. These similarities would make the assignment of efg tensors to bond sites ambiguous on the basis of structure alone. Fortunately, the evidence that the deuterons of sites 3, 4 and 5 undergo hindered rotation makes it possible to assign the efg tensors of sites 1 and 2 at 193^{o}K where the NMR spectra of the sites 3, 4, and 5 are merged.

The second principal component is found to lie approximately along the normal to the plane defined by N_1-N_2-D. The angles formed between the second principal component

and the normal to the plane of N_1-N_2-D are 17°, 16°, 14°, 12° and 5° for sites 1 through 5 respectively. The estimated error is ±3°, somewhat larger than for the first principal component because the efg tensors are nearly axially symmetric. Similar results have been found by Chiba[17] for the O-D...O bond. The slight change in the efg tensor orientation of the 1 and 2 site deuterons between 77°K and 193°K is smaller than the experimental error.

The spectrum observed at an orientation with $c \perp H_0$ and near $b \parallel H_0$ showed some evidence of a splitting of the lines corresponding to site 1. This may indicate that the deuteron of site 1 can be found at either of two almost identical positions. The only region of the rotation spectrum in which this splitting was evidenced is that corresponding to maximum splitting, for which the field H_0 is almost along the first principal axis of the field gradient tensor.

It was assumed that such a splitting might be associated with structural differences corresponding to ferroelectric domains in the crystal. Ordinarily the domains of opposite polarization of a ferroelectric are related by reflection. Observation of such a splitting as described would indicate that in LiHzS domains are not

related by reflection and might be considered a new type of ferroelectric. [14] An unsuccessful attempt was made to observe the effect of electric fields, of the order of 10^4 v/m, on the spectrum. The crystal was prepared by cutting and polishing faces perpendicular to the c axis. Silver contacts were then painted on these faces in the form of E in order to minimize rf currents. The signal to noise ratio was so degraded, by the introduction into the sample region of these polarizing plates, that the line splitting was no longer observed. The low temperature spectrum showed no other evidence of domain effects.

A sufficiently large number of hydrogen bonded systems of the type O-H...O have been studied to allow correlation of the coupling constant eqQ/h, with O...O bond lengths and with the O-H stretching frequencies ν_{OH}.[18] The number of similar studies of N-H...X systems is small. Table IV lists the coupling constant and other pertinent information for several such systems.

O...O bond lengths range from 2.40 Å to about 3 Å. The range [26] of N...O bond lengths is approximately 2.85 Å to 3.05 Å.* Although a plot of eqQ/h against bridge length

---

*These estimates do not include weak or bifurcated bonds for which the bridge length may be considerably longer.

TABLE III

N-H...X Bond Angles and Intra-bond Lengths Calculated from the Room Temperature Data of Padmanabhan and Balasubramanian.[11]

	N-H...X (H-bond) Bond Angle, Deg.	H-bond Dimensions, Å N-H	H...X	N——X
1	118.2	1.02	2.35	2.97
2	156.4	1.02	2.09	3.05
3	166.3	1.02	1.84	2.84
4	146.1	1.01	2.00	2.89
5	150.3	1.05	2.03	2.99

for O...O bonds shows a strong correlation, an attempt to correlate bridge length with eqQ/h for N-H...O bonds was not successful. Within the ND_3 group of LiDzS the dependence of eqQ/h on $(1/r_{N-D})^3$ is consistent. The slope of such a plot can be used to estimate the effective charge of the nitrogen nucleus in the crude approximation that no other nuclear site contributes to the efg at the

TABLE IV

Coupling Constants and Asymmetry Parameters for Some N-D Bonds.

Compound	Bond	Temperature	eqQ/H(kHz)	η	Reference
Urea d_4 single crystal	$N-D_1...O$	298°K	210.8±1	0.139±0.010	
	$N-D_2...O$	298°K	210.7±1	0.146±0.010	
	$N-D_2...O$	298°K	206.3±1.2	0.138±0.010	19
Glycine polycrystalline (bond types are conjectured)	N-D...O	150°K	168	0.00	
	N-D...O	150°K	188	0.00	
	ND_3 average	T>250°K	80	0.24	
	ND_3 average	T>250°K	71.2	0.40	20
Glycine single crystal (bond type is conjectured)			Principal component		
	ND_3 average	298°K	51.10	.22	
	ND_3 average	298°K	51.46	.22	21
$ND_4D_2PO_4$ single crystal	N-D...O	298°K	130	0.0	22
ND_4Cl single crystal	N-D...Cl	113°K	180.1±1.0	0.00±0.01	23
ND_3 polycrystalline	N-D...N	75°K	156 ±7		
	ND_3 average	185°K	72.5±.9		24
$(ND_4)_2SO_4$	N-D...O	77°K	180	0.0	25

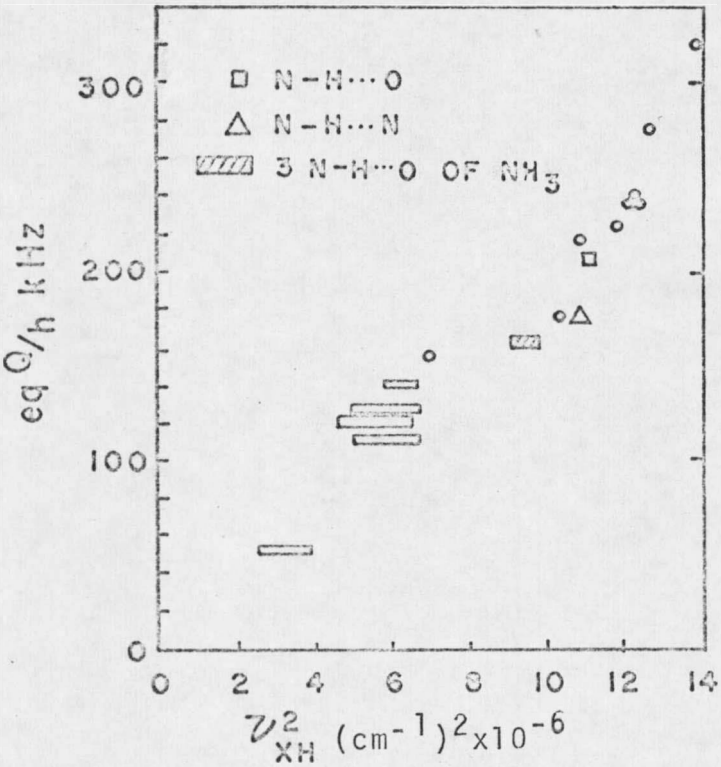


Fig. 8. Coupling Constant Plotted Against the Square of the X-H Stretching Frequency for O-H Bonds of a Number of Compounds Except for the N-H Bonds of LiHzS as Indicated. (After Blinc & Hadzi)[18]

deuteron. Such an estimate yields a value of 0.45e for the effective nuclear charge of the nitrogen.

Fig. 8 shows a plot of eqQ/h against the square of

the O-H and N-H[27,28] stretching frequencies. Bonds represented in the upper right region of the plot are O-H...O bonds of crystal hydrates, while the O-H...O bonds found in phosphates and selenites are represented in the lower left region. The stronger bonds of the crystal hydrates show a larger dependence on ν^2_{OH} than the bonds of the phosphates and selenites. The points corresponding to the nitrogen-hydrogen bonds of LiHzS fall near the transition between the two general O-H bonds represented in this plot.

CHAPTER III DEUTERON MOTION

CONDUCTIVITY AND DIELECTRIC CONSTANT.

An electrolysis experiment carried out by Vanderkooy demonstrates that the c axis conductivity in LiHzS is due to protons. Electrical conductivity measurements by Vanderkooy, Cuthbert and Petch[29] (hereafter referred to as VCP) show that the c axis conductivity is two to three orders of magnitude greater than conductivity in the a or b direction. Their experiments were carried out on crystal samples of approximately 8 mm thickness with electrodes of area about 0.5 cm^2. A dc voltage of 290 volts was applied to the sample and an electrometer was used to measure the current. Although care was taken to avoid measuring polarization currents by waiting a time after application of the voltage before measuring the current, no mention is made of the use of a guard ring circuit in the experiment. Values found for the conductivity in the a, b and c axis directions are given in Table V. The c axis conductivity as a function of temperature found by VCP is displayed in Fig. 9. It was found that the a and b axis conductivities could not be represented by a single activation energy over this temperature range.

The conductivities of LiHzS and LiDzS reported herein have been measured by a slightly different technique. The

TABLE V

Conductivities and Activation Energies for Normal and Deuterated Lithium Hydrazinium Sulfate

$\sigma(\Omega\ cm)^{-1}$ Measured at Room Temp	E Activation (eV)	Compound	Axis Measured Along	Reference
$0.93\pm0.09\times10^{-11}$		LiHzS	a	VCP
$0.80\pm0.09\times10^{-11}$		LiHzS	b	VCP
$0.23\pm0.09\times10^{-8}$	0.85	LiHzS	c	VCP
0.4×10^{-12}	0.34	LiHzS (Irregular Sample)	a	
0.15×10^{-12}	0.58	LiDzS	a	
0.4×10^{-12}	0.47	LiDzS	b	
0.12×10^{-9}	0.65	LiDzS	c	
0.10×10^{-8}	0.51	LiHzS	c	

experiment is described in Chapter IV. The room temperature conductivities for deuterated and undeuterated crystals are given in Table V. Activation energies are also given. These are somewhat lower for LiHzS than those found by VCP. In addition the a and b axis conductivities of the

deuterated compound were measured. Although they could not be described by a single activation energy over the entire temperature range studied, the data between room temperature and about 110°C appeared linear and was best fit to get an estimate of the activation energy for this region. Two a axis and one b axis studies were used, giving the activation energies indicated in Table V. Above 170°C all three of these log conductivities vs 1/T curves indicate activation energies of more than 1.5 eV. The c axis log conductivity vs 1/T curve has a constant slope over the entire temperature range and the best fit to this is shown in Fig. 9.

The dielectric constant of LiDzS has been measured in this laboratory. The results of these measurements are displayed in Figs. 10, 11 and 12. Pepinsky et al,[10] who first examined the dielectric constant of the crystal, found no anomaly in the dielectric constant between -196°C and 140°C. Our study has shown no dielectric peak up to 205°C.

According to the Debye* equations $\varepsilon' \propto 1/(1 + \omega^2\tau^2)$ and $\varepsilon'' \propto \omega\tau/(1 + \omega^2\tau^2)$. Log ε' and log ε'' plotted as

---

*A discussion of the dielectric loss may be found in Chapter II, Dielectric Behavior and Structure by Charles Phelps Smyth, McGraw Hill Book Co., Inc., New York, 1955.

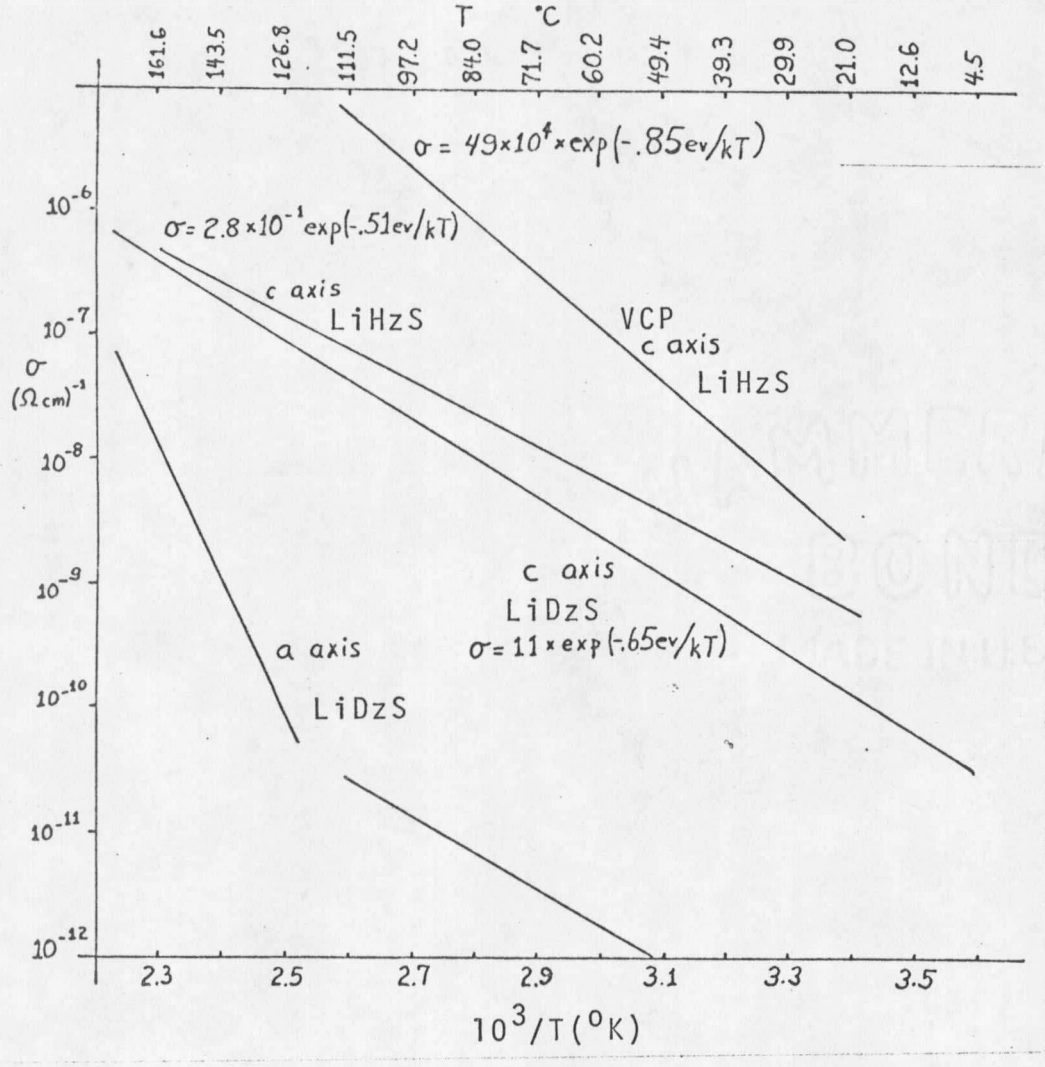


Fig. 9. Best Fit Curves of the Logarithm of Conductivity for LiHzS and LiDzS as a Function of Temperature. (VCP Indicates Results from Reference 29.)

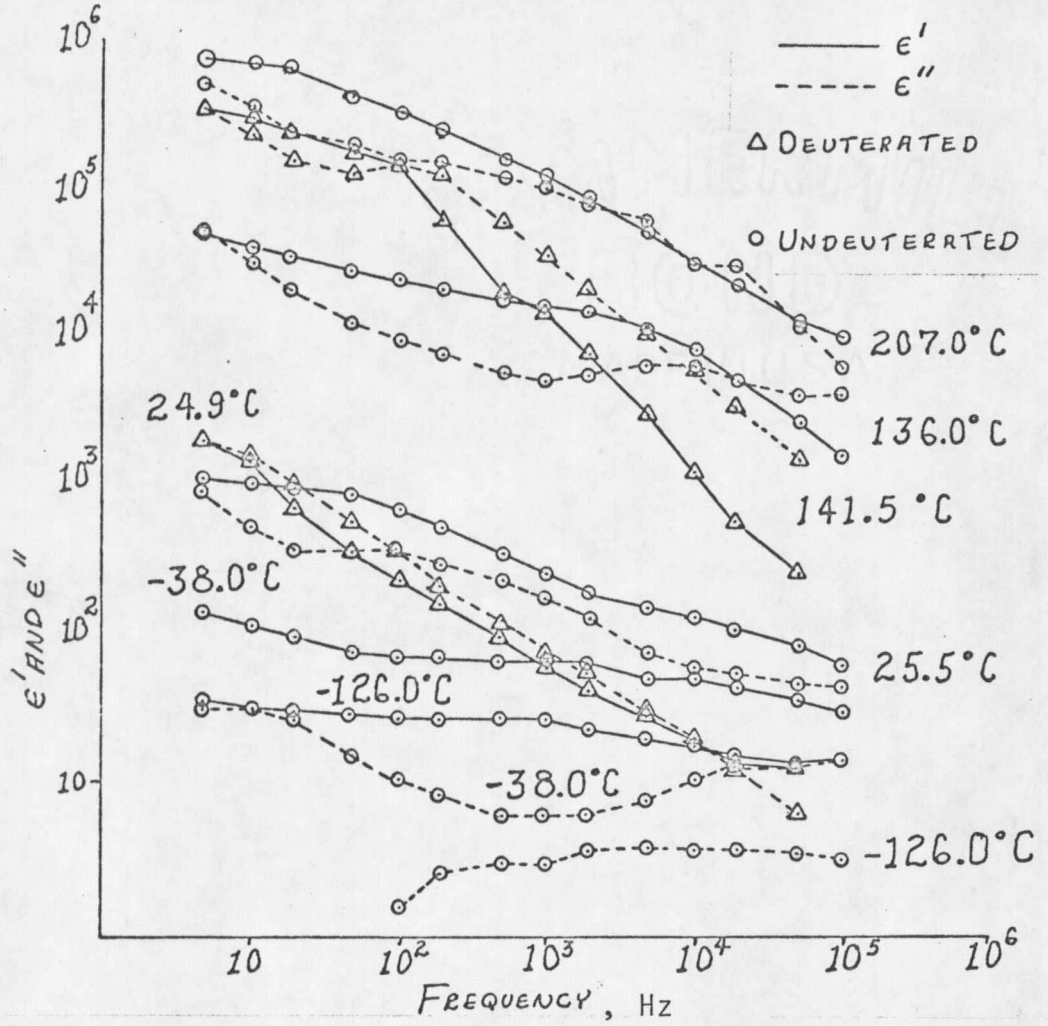


Fig. 10. Logarithm of the Real and Imaginary Parts of the Dielectric Constant for LiHzS and LiDzS Measured Along the c Axis vs Frequency at which the Measurement Was Made.

functions of ω for several fixed temperatures show negative slopes near -0.5, as shown in Fig. 10. This behavior is not consistent with the Debye equations, which result from the assumption of a single relaxation time τ. It agrees quite well with the assumption of a distribution $y(\tau)$ of relaxation times in the relations

$$\varepsilon' = \varepsilon_\infty + \int_0^\infty \frac{y(\tau)d\tau}{1+\omega^2\tau^2}, \qquad \varepsilon'' \int_0^\infty \frac{\omega\tau y(\tau)d\tau}{1+\omega^2\tau^2},$$

if $y(\tau) = (a-1)\tau_m^{a-1}[\varepsilon(0)-\varepsilon_\infty]\tau^{a-1}$ for $0<\tau<\tau_m$, and $y(\tau) = 0$ for $\tau>\tau_m$. For this $y(\tau)$, if $\omega\tau_m>>1$, the dielectric constant becomes

$$\varepsilon = \varepsilon'-j\varepsilon'' = \varepsilon_\infty + \frac{\pi(a-1)[\varepsilon(0)-\varepsilon_\infty]}{2(\omega\tau_m)^2}\left[\frac{1}{\sin\frac{a\pi}{2}} - \frac{j}{\sin\frac{(a+1)\pi}{2}}\right]$$

The Cole-Cole plot of ε'' versus ε' in Fig. 11 shows that LiDzS almost obeys this expression at 25°C for a = 0.5. A more concentrated distribution of relaxation times is exhibited by the curve for LiHzS at room temperature, for which the contribution $\sigma_{dc}/\varepsilon_0\omega$ to ε'' made by the dc conductivity mechanism has been subtracted out. A single relaxation time would give a semicircle centered on the ε' axis.

Activation energies for the relaxation mechanism are estimated from Fig. 12. For the deuterated compound two contributions are evident, a low temperature contribution of 0.4 eV and a contribution of 0.7 eV in the temperature region above 100°C.

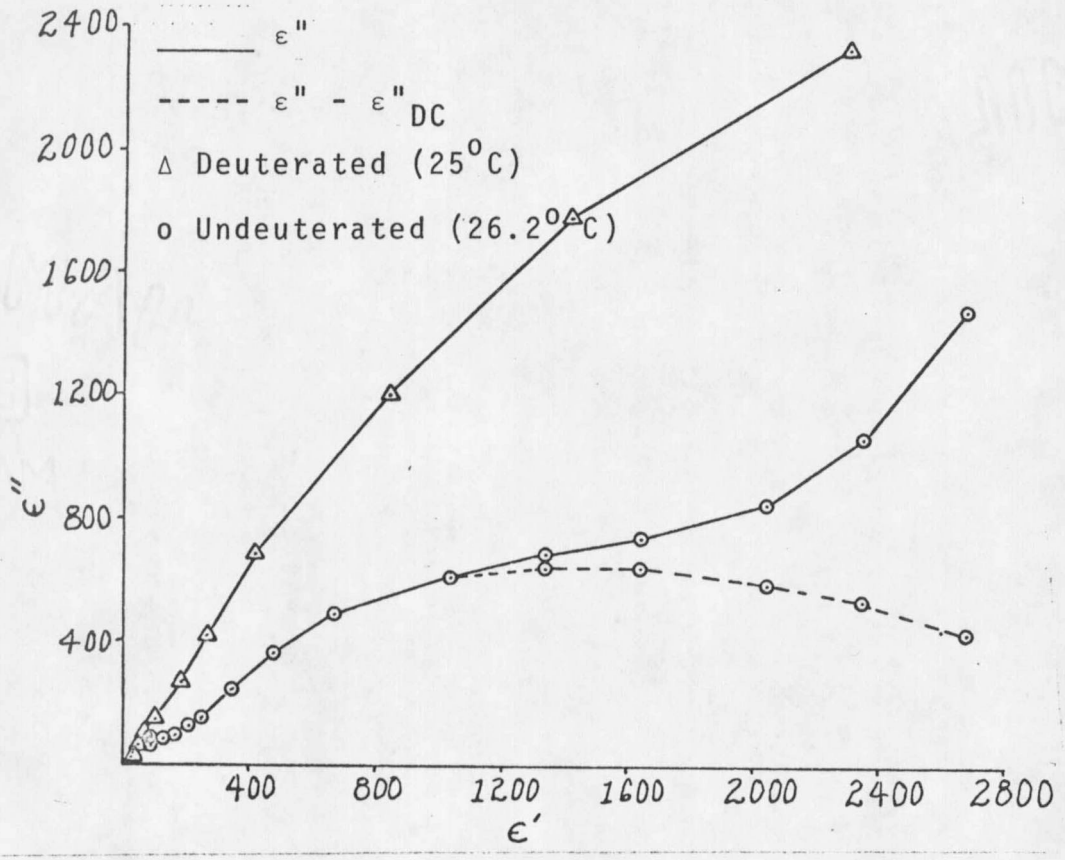


Fig. 11. ε" vs ε' for LiHzS and LiDzS.

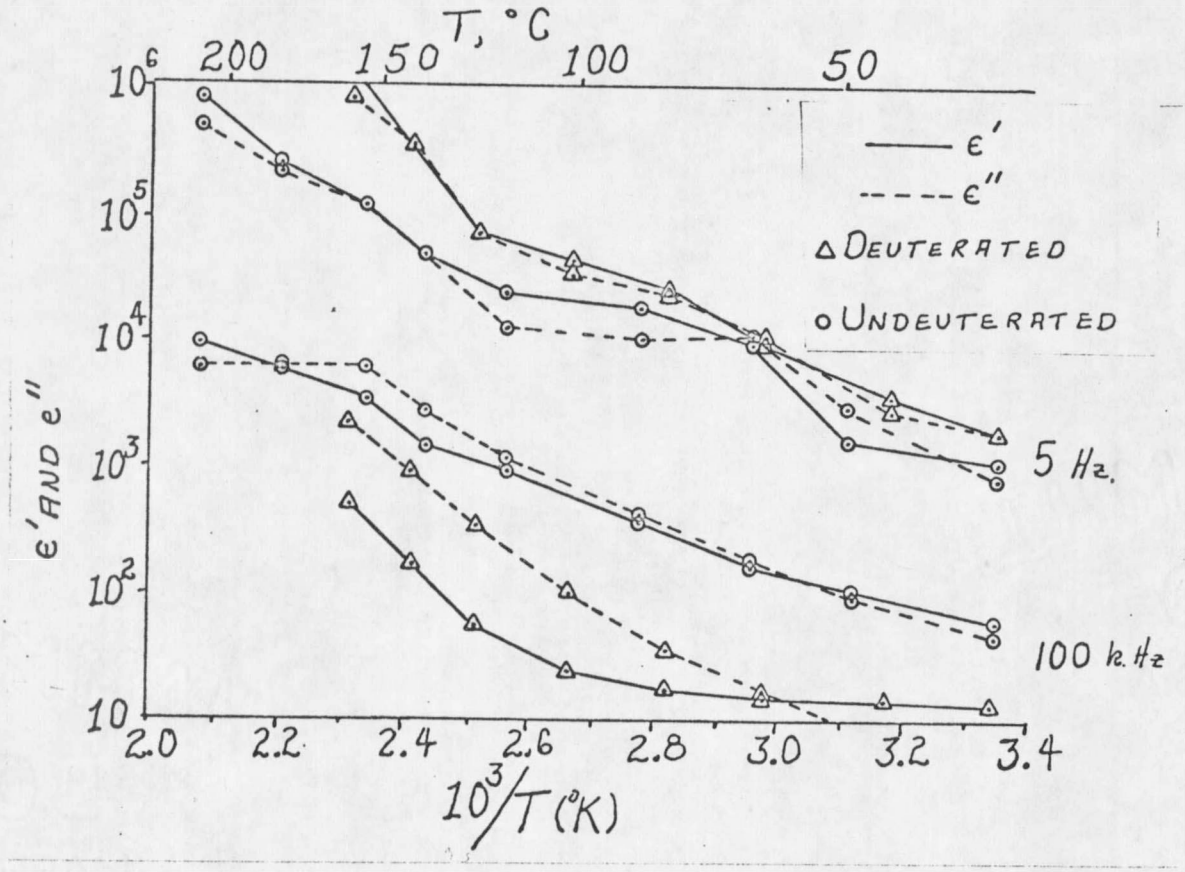


Fig. 12. Logarithm of the Real and Imaginary Parts of the Dielectric Constant for LiHzS and LiDzS Measured Along the c Axis as a Function of Temperature.

PREVIOUS NMR STUDIES.

Two previous NMR studies have been carried out on $LiHzS$.[12,13] In the first of these, the second moment of the protons and the quadrupolar splitting of Li^7 were measured. In the later work, the second moment measurements of the first work were extended and the spin lattice relaxation time of the protons was measured. The first study of the second moment was carried out before the neutron structure study was done. On the basis of the second moments measured at various temperatures in powder samples and in single crystals at various orientations, the arrangement of the protons was deduced and the NH_3 and NH_2 motions were hypothesized. Fig. 13 shows the proton second moment as a function of temperature along the Li^7 satellite separation. Because of the change in the satellite separation, Cuthbert and Petch[12] suggest that the crystal undergoes a gradual structural change which is complete at about 165°C.

The reduction in the second moment between liquid air temperature and 80°C was attributed to the onset of hindered rotation of the NH_3 group. The further reduction between 20° and 150°C was thought due to whatever mechanism provided exchange between sites 1 and 2. The final drop in second moment to the very low value of about 0.5 $gauss^2$ at 200°C

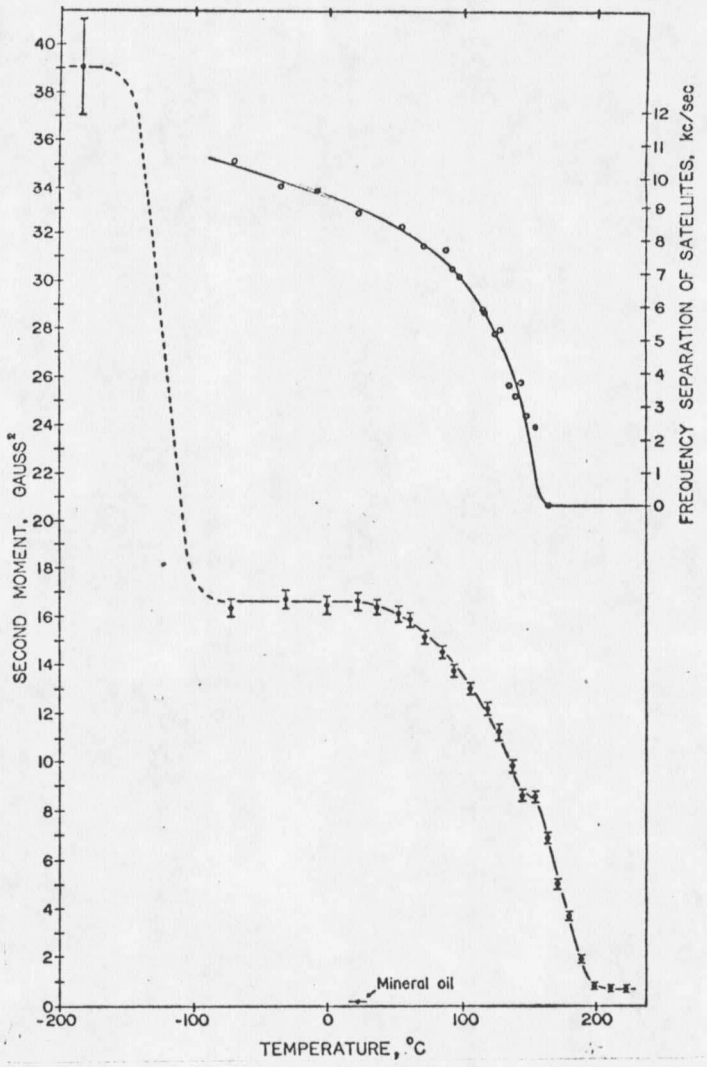


Fig. 13. The Open Circles Give the Variation with Temperature of the Frequency Separation Between the Two Li^7 Satellites Which Occur on the Same Side of the Central Line and Coincide in the High Temperature Polymorph of Lithium Hydrazinium Sulfate. The Solid Circles Give the Variation with Temperature of the Second Moment of the Proton Resonance in Powdered LiHzS. (After Reference 12)

was thought to be due to either rapid diffusion of the protons through the crystal or to tumbling of the entire N_2H_5 group. These authors suggest that the ferroelectric property of the crystal is associated with ordering of the N-H...N-H... chains(Fig. 2). It was then pointed out that on the basis of this model, exchange between sites 1 and 2 would lead to a loss of order of these N-H dipoles and hence a ferroelectric transition.

The second moment measurements presented in the later study are in general agreement with those of the earlier, although the knee in the curve at about 8.8 gauss^2 was not repeated (Fig. 14). The spin lattice relaxation time of the protons was measured. Fig. 15 shows a plot of T_1 vs 1/T. Below a temperature of about 190^{o}K the relaxation is attributed to molecular reorientation of the NH_3 group with activation energy 0.182 ± 0.013 eV. It is assumed that above about 60^{o}C the NH_2 reorientation mechanism is responsible for the decrease in T_1 and the activation energy is found to be 0.43 ± 0.09 eV.

In summary, the second moment studies of the protons suggest that the protons of sites 3, 4 and 5 undergo a hindered rotation, and that this motion becomes important in the temperature range between 100 and 150^{o}K. The protons of sites 1 and 2 begin to undergo some sort of

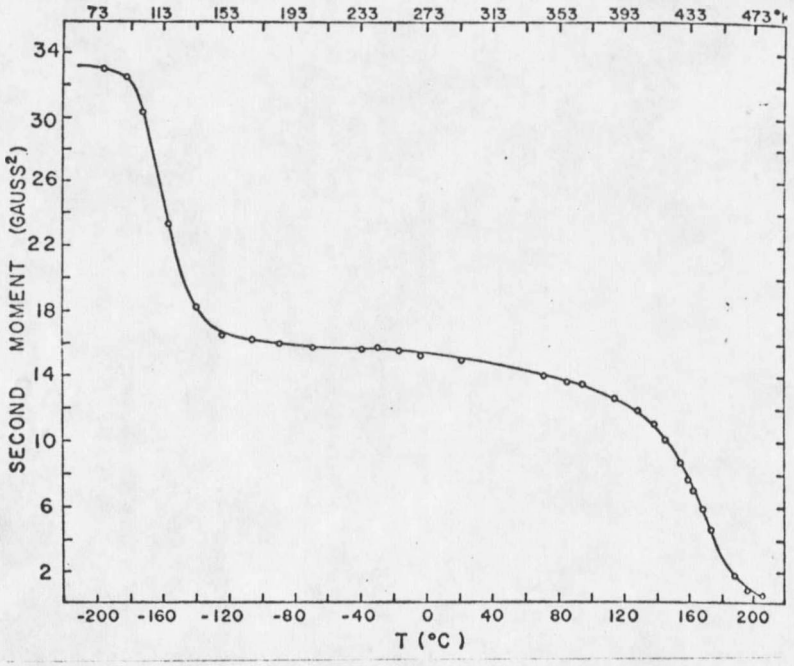


Fig. 14. Temperature Dependence of the Second Moment of the Proton Absorption Signal from Powdered LiHzS. (After Reference 13)

exchange between sites in the region near 0°C. Above 150°C either a very rapid diffusion of protons between N_2H_5 groups starts to occur or else the groups themselves begin to tumble and translate through the crystal. The T_1 measurements yield activation energies for the rotations. Li^7 quadrupolar splitting studied as a function of

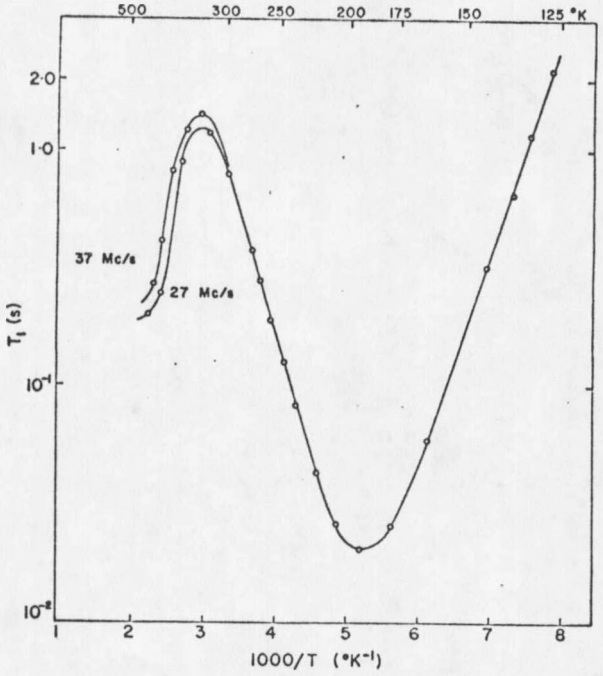


Fig. 15. Temperature Dependence of the Proton Spin Lattice Relaxation Time T_1 in Lithium Hydrazinium Sulfate. (After Reference 13)

temperature implies a structural change to a higher symmetry form which is complete near 165°C.

HIGH TEMPERATURE SPECTRUM.

If the quadrupolar interaction is a perturbation on the Zeeman interaction as in these experiments, when a deuteron changes sites its energy level scheme is changed if there is a change in the electric field gradient component parallel to H_0. When the rate of site change becomes large enough, the spectral lines corresponding to individual sites are broadened and disappear. If the exchange frequency becomes higher still, a new pair of spectral lines may appear, corresponding to an efg which is the average over the sites between which the jumping occurs.

Evidence discussed in the previous section indicates that protons in the NH_2 and NH_3 sites undergo hindered rotation. By studying the NMR spectra of deuterons in LiDzS it has been possible to determine unambiguously the type of motion taking place, along with estimates of the frequency of the motion, and the activation energies involved.

When the deuteron NMR spectrum (Fig. 16) of LiDzS is studied as a function of temperature it is found that the lines in a spectrum corresponding to sites 3, 4, and 5 broaden and vanish near $110^{o}K$. As the temperature is further increased a new pair of lines appear near $140^{o}K$. These lines are very strong and are still in evidence at $465^{o}K$. The splitting of these lines as a function of the



Fig. 16. NMR Spectra Taken with b|| H_o at Temperatures Indicated.

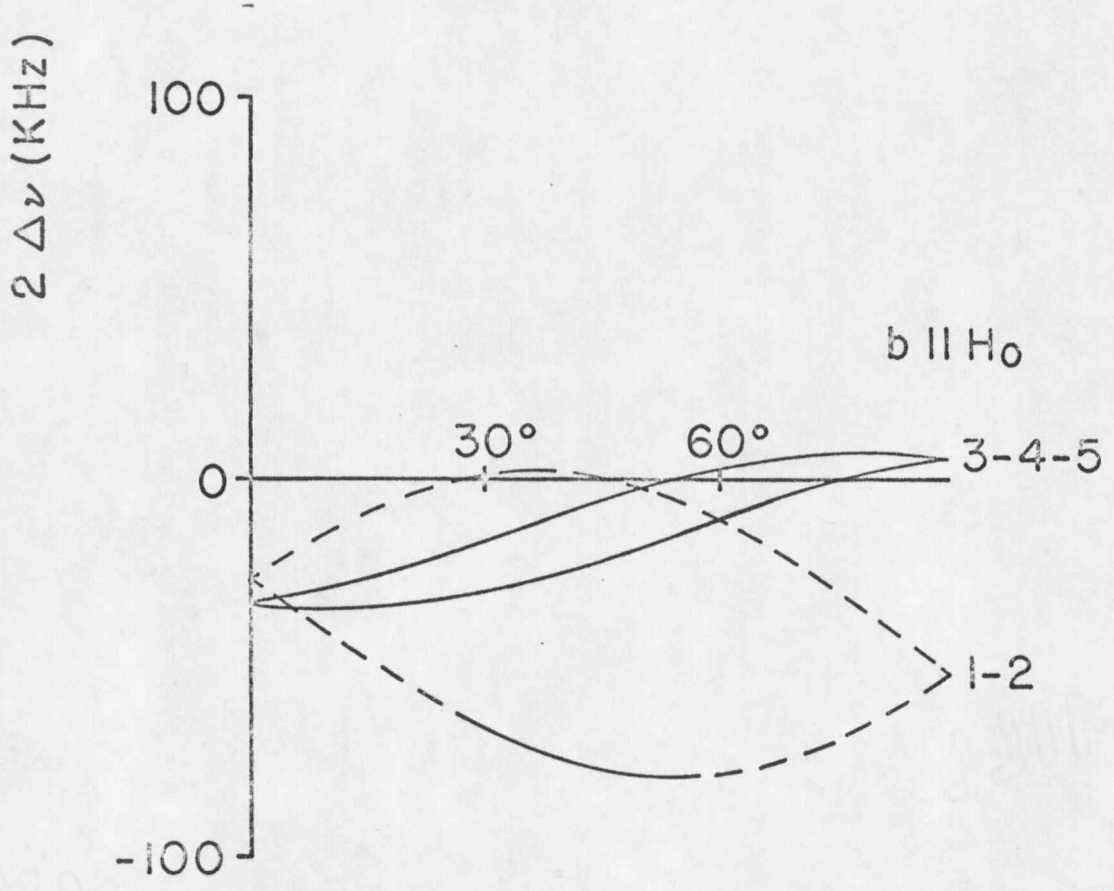


Fig. 17 Quadrupole Splitting Patterns of the Two Sets of Averaged Lines for Rotation about the a Crystallographic Axis at 95°C. Dashed Lines Indicate Regions in which the Spectral Lines Could not be Observed.

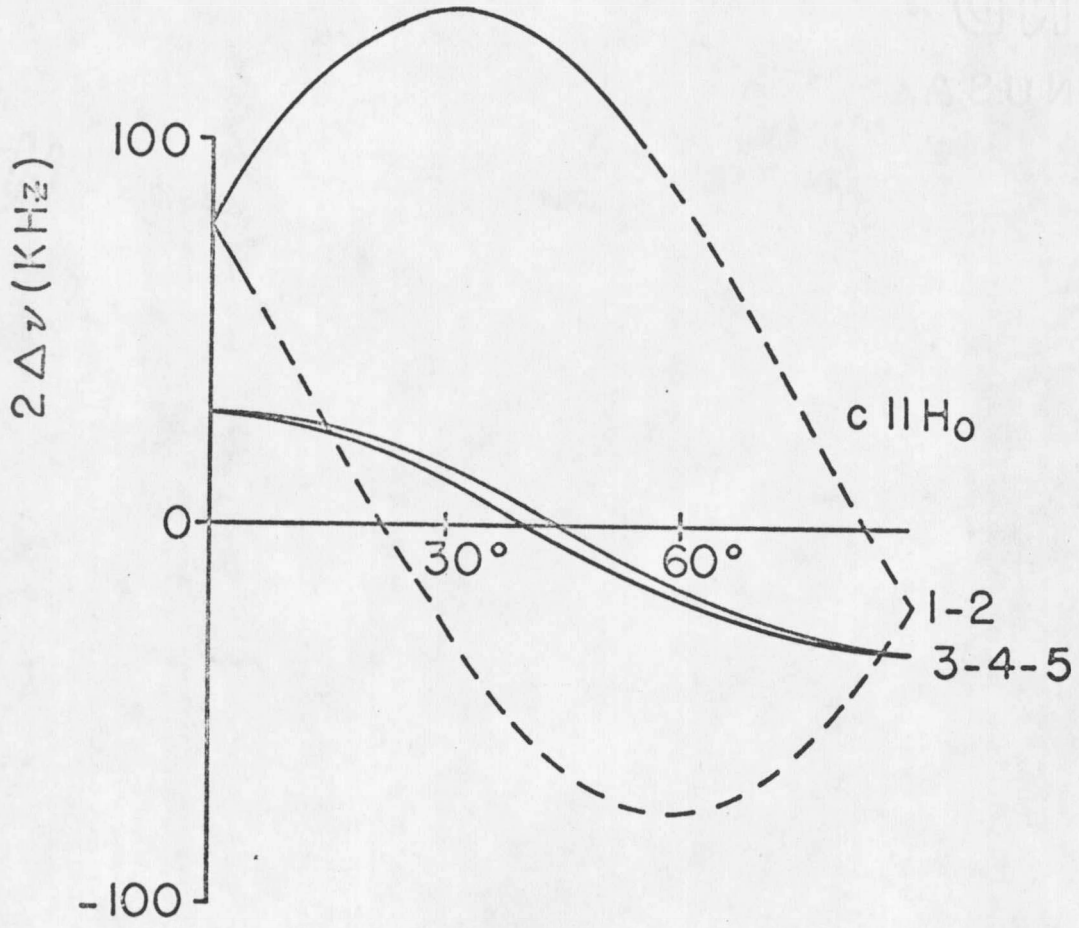


Fig. 18 Quadrupole Splitting Patterns of the Two Sets of Averaged Lines for Rotation about the b Crystallographic Axis at 95°C. Dashed Lines Indicate Regions in which the Spectral Lines Could not be Observed.

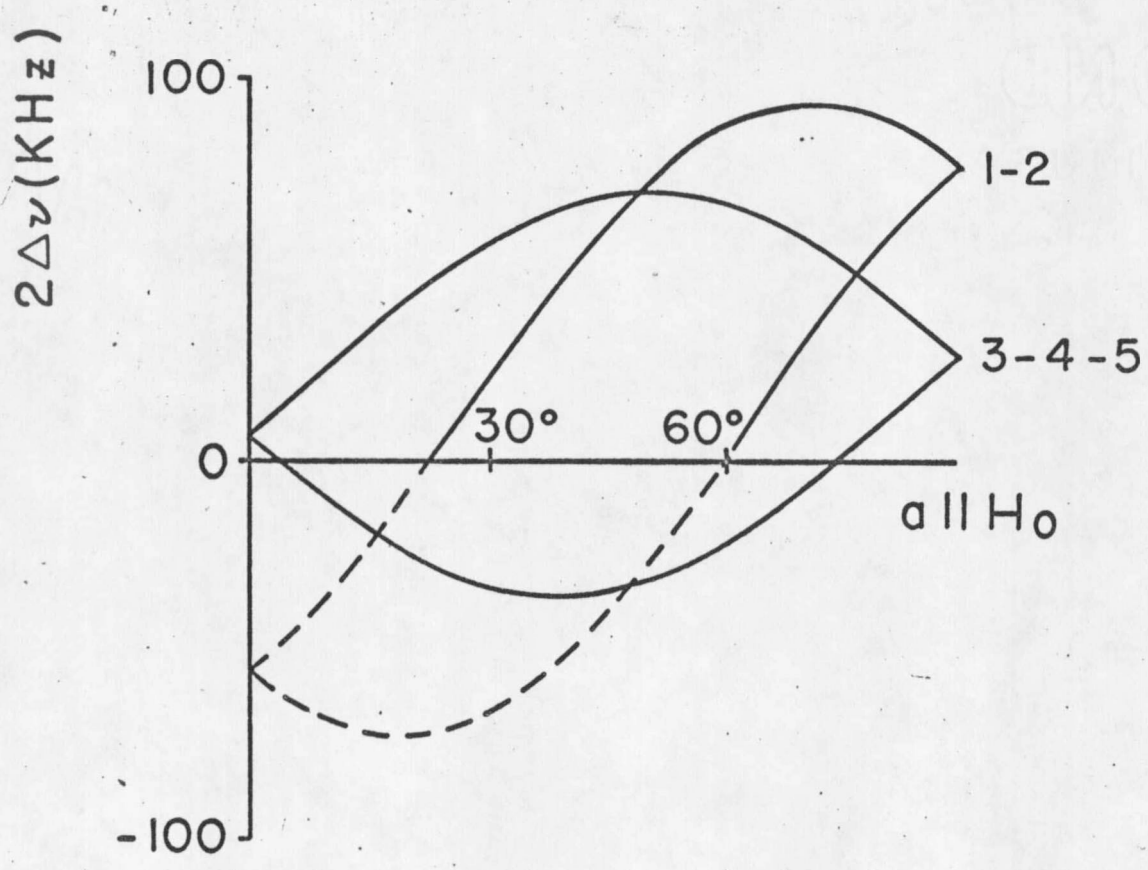


Fig. 19 Quadrupole Splitting Patterns of the Two Sets of Averaged Lines for Rotation about the c Crystallographic Axis at 95°C. Dashed Lines Indicate Regions in which the Spectral Lines Could not be Observed.

angle between crystal axis and magnetic field is shown in Figs. 17, 18, and 19. Near 285°K, the lines in the spectrum corresponding to sites 1 and 2, broaden and disappear. A new pair of lines, due to the average of sites 1 and 2, appears at about 330°K. These lines, however, are not evident for all orientations of the crystal relative to H_0. Figs. 17, 18 and 19 show the splitting for these lines, indicating as well the angular region in which the lines are not observed.

The complete rotation spectrum of the deuterons was studied at 193°, 298°, 338°, 368°, and 438°K. Because the spectrum is not sensitively dependent on the temperature, a variation of ±5°C was allowed. This produced variations in the spectrum well within experimental error. The results of these measurements are tabulated in Table VI.

The values of eqQ/h for the averages over sites 3, 4, and 5 show a consistent decrease of about 10% from -80°C to 165°C. If all the contents of the unit cell were to expand at the same rate, the efg would vary as (lattice parameter)$^{-3}$. Using the average of the anisotropic thermal expansion coefficients,[30] this temperature yields an efg decrease of about 2.5% from -80°C to 165°C. Two possible origins for the remainder of the decrease are the increase with temperature in the amplitude of the torsional

TABLE VI

Coupling Constant eqQ/h, Asymmetry Parameter η, and the Angles Between the First Principal Axes and the Crystallographic Axes for the efgs Resulting from Motional Averaging over Sites 1 and 2 and over Sites 3, 4 and 5. Calculated Averages Based on efgs Measured at 78°K for Individual Sites Are Given for Comparison.

	Temperature	eqQ/h, kHz	η	θ_x	θ_y	θ_z
				(error, all angles ± 0.5)		
	-80°C	48.9 ± 0.5	0.29 ± 0.05	37.1	127.4	89.0
Measured for average due to sites 3, 4 and 5	25°C	48.6 ± 0.5	0.22 ± 0.05	38.0	127.5	89.9
	65°C	47.5 ± 0.5	0.18 ± 0.05	38.4	128.3	88.4
	95°C	46.3 ± 0.5	0.16 ± 0.05	39.1	129.0	87.6
	165°C	44.0 ± 0.5	0.20 ± 0.05	40.1	130.0	87.5
Calculated average for sites 3, 4 and 5		51.0	0.46	36.9	126.7	88.5
Measured for average due to sites 1 and 2				(error, all angles ± 2.0)		
	95°C	91.0 ± 3	0.90 ± 0.15	64.0	52.0	131.0
	165°C	89.4 ± 3	0.75 ± 0.15	64.1	61.3	139.5
Calculated average over sites 1 and 2		97.8	0.98	64.2	45.8	124.8

oscillations of the ND_3 groups, and the structure change indicated by the decrease in the difference between the quadrupolar splittings of the two Li^7 sites. The direction of the first principal axis of the ND_3 group average forms an angle of 3.6^o at room temperature, 2.6^o at 95^oC and about 1^o at 165^oC with the N_1-N_2 direction as calculated from the neutron diffraction data obtained at room temperature.

A somewhat similar ND_3 group has been studied in glycine (Table IV). This group is of the form C-ND_3 as opposed to the N-ND_3 found in LiDzS. The coupling constant for the glycine ND_3 average is between 70 and 80 kHz as compared to 48.6 kHz in LiDzS at 25^oC. The asymmetry parameter for the group in glycine is 0.22 as compared to 0.22 ± 0.05 in LiDzS. This would suggest that either the effective charge of the nitrogen in a N-N bond is less than that in an N-C bond or that the N-D distances are greater in LiDzS than in glycine, or a combination of these two.

The efg resulting from motional averaging over bonds 1 and 2 did not change measurably between 65 and 95^oC. The efg at 165^oC showed a change and its coupling constant, asymmetry parameter, and angles are given in Table VI. Because of the limited angular range over which these lines could be observed, the estimated error is larger than for

the D_3-D_4-D_5 average. At 95°C the first principal axis of the D_1-D_2 average lies within 2° of the plane defined by H_1-N_1-H_2 and within 4° of the line bisecting the H_1-N_1-H_2 angle.

Values of the coupling constant, asymmetry parameter, and the angles between the first principal axis and the crystal axes are given in Table VI for a calculated average over sites 1-2 and over sites 3-4-5. This calculated average is obtained from an efg whose components in the crystal frame are the sums of the components of the efg tensors for the individual sites in the crystal frame divided by the number of sites. The agreement between the calculated averages and the values obtained at lowest temperature measured is good. The type of motion which gives rise to these averages can be understood from the measurements discussed above. The ND_3 exchange takes place symmetrically about the N-N axis by means of hindered rotation through 120° steps as was suggested by Cuthbert and Petch[12]. The D_1, D_2 averaging takes place by interchange between sites 1 and 2 bonded to the same nitrogen. This does not indicate a rotation about the N-N bond direction as had previously been suggested as a possible motion.[13]

EXCHANGE PROBABILITY.

Abragam[8] discusses a general method for calculating the exchange probability per unit time, Ω, for nuclear exchange between sites from a knowledge of the line width. Since in principle the technique is applicable to the case of jumping between any number of nuclear sites, it is possible to estimate the exchange probability as a function of temperature and also the activation energy for the exchange of deuterons of both ND_2 and ND_3 sites. Chiba[31] has applied a similar method to the case of D_2O in $Ba(ClO_3)_2 \cdot D_2O$.

The calculation of the relation between intersite exchange probability and line width is based on the following assumptions. The probability that the Larmor frequency of the nucleus, ω, has a value ω_2 at the time $t' = t + \Delta t$ when it is known that it had a value ω_1 at time t is:

1. independent of the values of ω prior to t
2. dependent on the times t and t' only through the difference $t' - t = \Delta t$ and can accordingly be written as $W(\omega_1 | \omega_2, \Delta t)$.

The absorption

$$I(\omega) = re \int_0^\infty G(t) e^{-i\omega t} dt \qquad (3.1)$$

is obtained by calculating the relaxation function

$$G(t)=\langle \exp\{i\int_{o}^{t}\omega(t')dt'\}\rangle . \qquad (3.2)$$

It is found that

$$G(t)=\overline{W}\cdot\exp\{(i\overline{\omega}+\overline{\pi})t\}\cdot\overline{1}, \qquad (3.3)$$

which makes

$$I(\omega)=re\{\overline{W}\cdot A^{-1}\cdot\overline{1}\} . \qquad (3.4)$$

W is a vector whose components, W_α, are the probabilities that at any time t the frequency of the system is ω_α. A^{-1} is the inverse of the matrix

$$A=i(\overline{\omega}-\omega\overline{1})+\overline{\pi} \qquad (3.5)$$

where $\overline{\omega}$ is a diagonal matrix with components $(\omega)_{\alpha\beta}=\omega_\alpha\delta_{\alpha\beta}$, $(\pi)_{\alpha\beta}=\pi(\omega_\alpha,\omega_\beta)$ the probability of transition between levels ω_α and ω_β, $\overline{1}$ a unit matrix, and ω a constant. A is of rank n where n is the number of deuteron sites among which jumping occurs. The matrices

$$\overline{\pi}=\begin{pmatrix}\Omega- & \Omega\\ \Omega & -\Omega\end{pmatrix} \qquad (3.6)$$

and

$$\overline{\omega}=\begin{pmatrix}\omega+\delta & o\\ o & \omega-\delta\end{pmatrix} \qquad (3.7)$$

where 2δ is the line separation (see Fig. 20) give for the

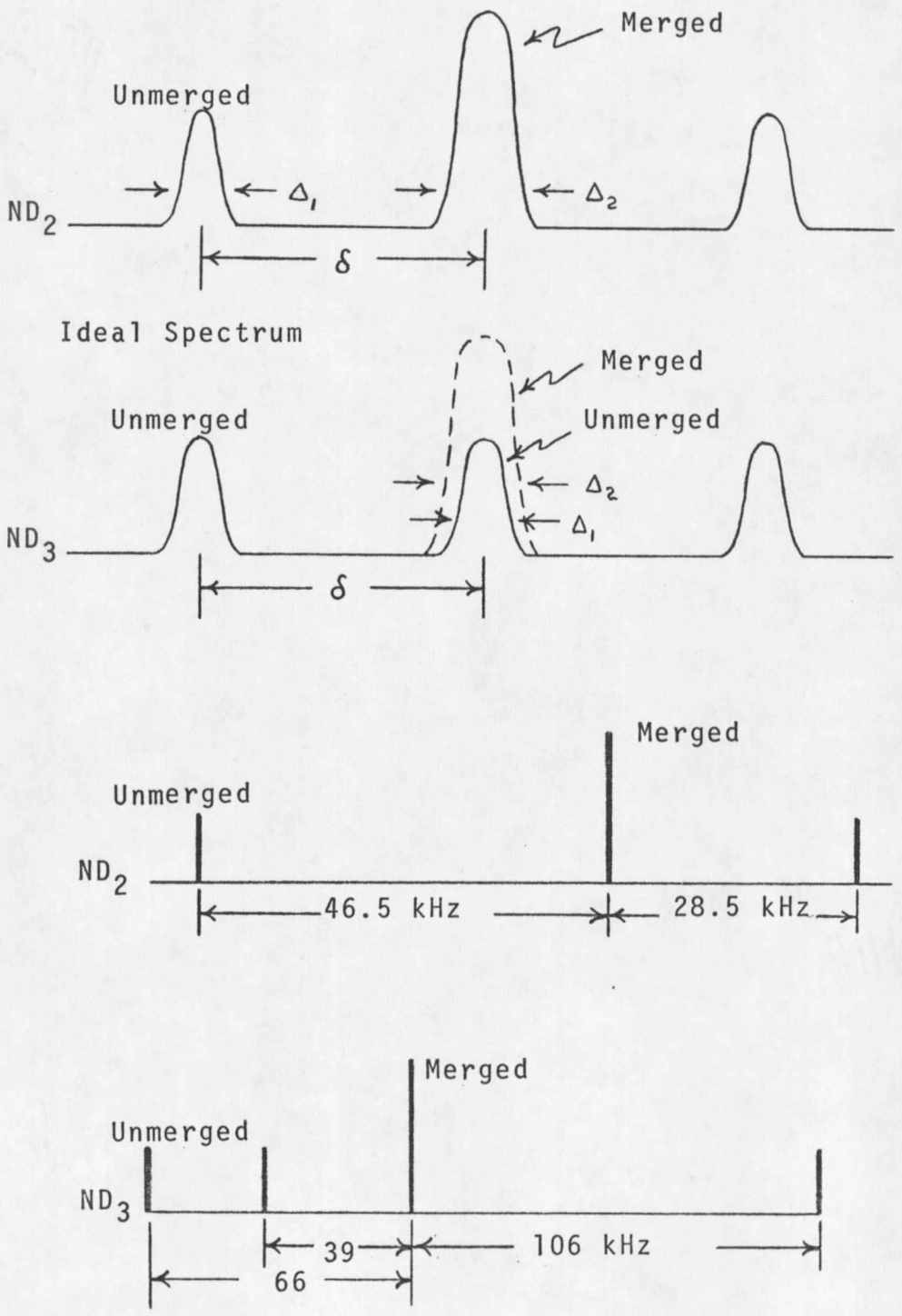


Fig. 20. Ideal and Observed D_3 and D_2 NMR Spectra.

ND_2 case

$$A = \begin{pmatrix} i(\omega+\delta+i\Delta)-\Omega & \Omega \\ \Omega & i(\omega-\delta+i\Delta)-\Omega \end{pmatrix}, \qquad (3.8)$$

where Δ is the unbroadened line width.
The resulting absorption for the ND_2 case is

$$I(\omega) = re\left\{ \frac{i\left[(-\omega+\delta-i\Delta)-(\omega+\delta+i\Delta)\right]-4\Omega}{(\delta^2+\Delta^2-\omega^2)-2\Delta\Omega+2i\omega(\Omega-\Delta)} \right\} . \qquad (3.9)$$

For the ND_3 case the matrices

$$\bar{\pi} = \begin{pmatrix} -\Omega & \Omega/2 & \Omega/2 \\ \Omega/2 & -\Omega & \Omega/2 \\ \Omega/2 & \Omega/2 & -\Omega \end{pmatrix} \qquad (3.10)$$

and

$$\bar{\omega} = \begin{pmatrix} \omega+\delta & o & o \\ o & \omega & o \\ o & o & \omega-\delta \end{pmatrix} . \qquad (3.11)$$

yield

$$A = \begin{pmatrix} i(\omega+\delta+i\Delta)-\Omega & \gamma & \gamma \\ \gamma & i(\omega+i\Delta)-\Omega & \gamma \\ \gamma & \gamma & i(\omega-\delta+i\Delta)-\Omega \end{pmatrix} . \qquad (3.12)$$

Δ is the unbroadened line width and $\gamma=\Omega/2$. The absorption is then calculated to be (3.13)

$$I(\omega)=\mathrm{re}\left\{\frac{3i\omega(\Omega+2\Delta)-3\Omega\Delta-(3\Omega/2)^2-\delta^2+3\omega^2-3\Delta^2}{i\left[-\omega^3+3\omega\Delta^2+\omega\delta^2+(9/4)\Omega^2\omega+6\Omega\omega\Delta\right]+\left[3\omega^2\Delta-\Delta^3-\delta^2\Omega+3\Omega\omega^2-3\Omega\Delta^2-(9/4)\Omega^2\Delta\right]}\right\}.$$

The low temperature spectrum observed for the ND_2 group consists of two lines split by 75 kHz (Fig. 20). For the ND_3 group three lines are involved and the line separation is indicated in Fig. 20. $I(\omega)$ is approximated for two limiting cases, $\Omega<<\delta$ (low temperature) and $\Omega>>\delta$ (high temperature) and from the resulting relations the line width is identified.

The ND_2 line widths are:

$W_{LT} = \Omega + \Delta$ Low Temperature

$W_{HT} = (\delta^2/2\Omega) + \Delta$ High Temperature

The ND_3 line widths are:

$W_{LT} = \Omega + \Delta$ Low Temperature

$W_{HT} = 4/9\ \delta^2/\Omega + \Delta$ High Temperature

These expressions are then solved for Ω. The line width value, W, is obtained by measuring the signal to noise ratio (S/N) as a function of temperature. The line width is assumed to be the reciprocal of the quantity $C(T/T_o)(S/N)$ where T/T_o compensates for the decrease in population difference and hence S/N with increasing temperature T. For the ND_2 group the constant C is obtained from the value ($2.3 \times 10^4/sec^{-1}$) of the line width at a temperature low enough to insure no line broadening due to the motion of interest. The width of the merged line is approximately the same so the same value of C is used for both the high and low temperature cases. The line width for the ND_3 group merged lines is larger ($3.9 \times 10^4/sec^{-1}$) than that for the unmerged lines so a different value of C was used for the high temperature than for the low temperature. The value of δ used in the calculation for ND_3 group was obtained by taking the average of the separation of the three unmerged lines giving $\delta \simeq 110$ kHz. The value of δ used in the calculation for the ND_2 group was taken to be half the splitting of the two unmerged lines (see Fig. 20). The resulting values of Ω are plotted against 1/T in Figs. 21, 22. The ND_2 data for the unmerged and merged regions is fitted to the line shown yielding an activation energy for the ND_2 motion $E_a = .46eV$.

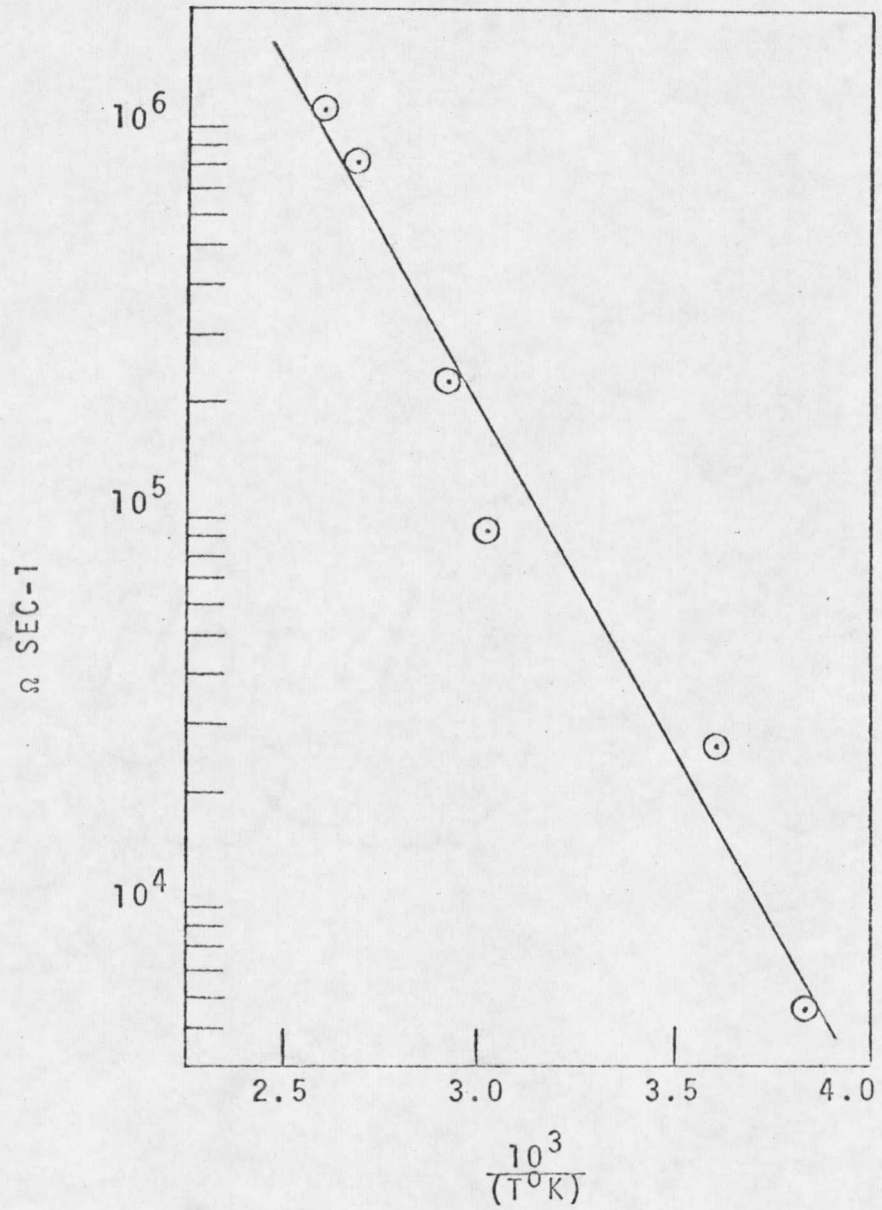


Fig. 21. Temperature Dependence of the Exchange Probability Ω for Exchange Between Deuteron Sites 1 and 2.

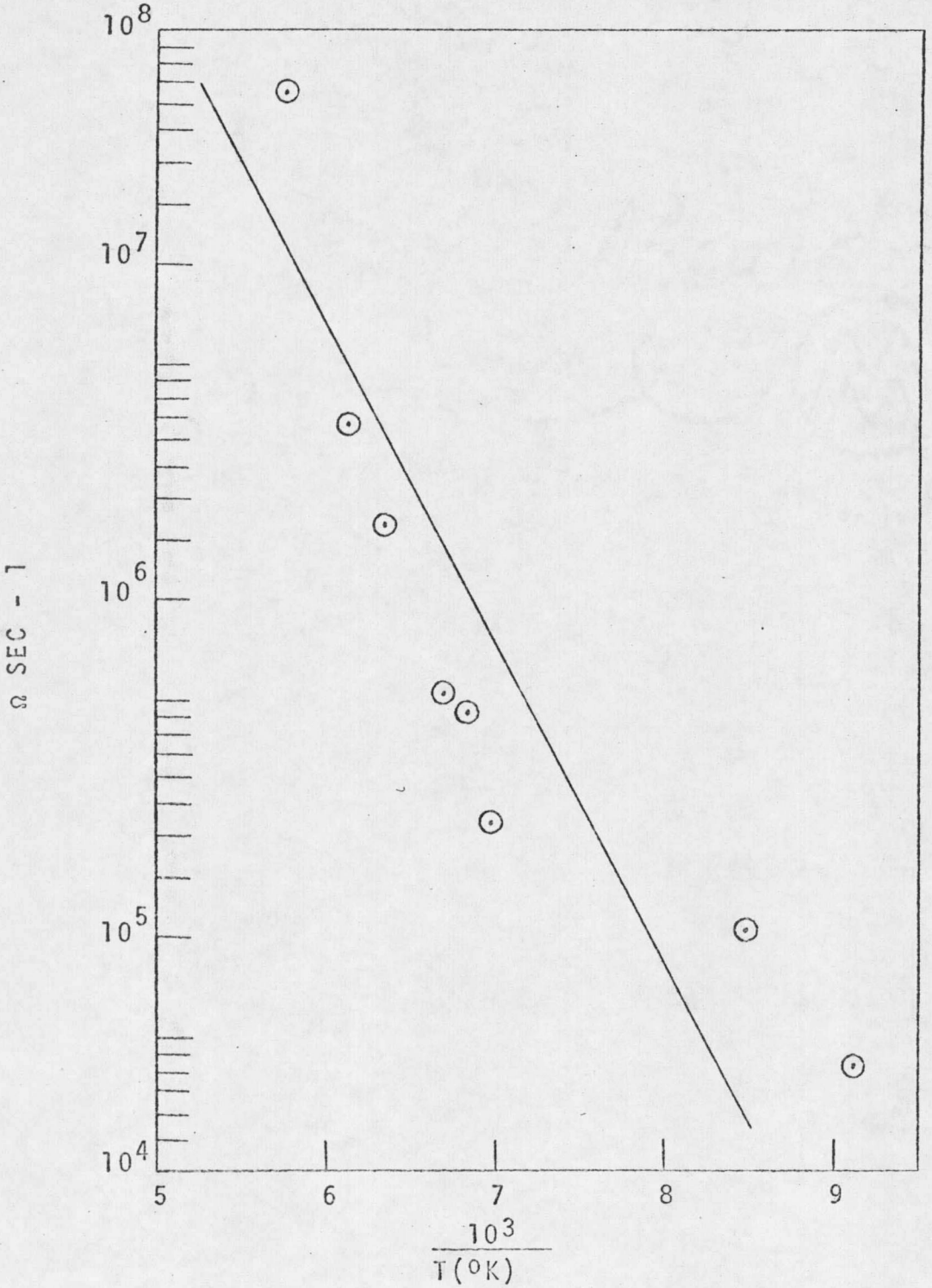


Fig. 22. Temperature Dependence of the Exchange Probability Ω for Exchange Between Deuteron Sites 1, 2 and 3.

The ND_3 data for the merged lines shows a much steeper slope than for the unmerged region. The straight line shown in Fig. 22 corresponds to an activation energy of .19eV, and approximates a best fit to the data shown.

The method discussed in this section is not as dependable a technique for determing the activation energy for such motion as is the measurement of the deuteron spin-lattice relaxation time, T_1. The slope of the curve Ω versus 1/T is dependent on both the line splitting δ and the line width Δ. The value chosen for δ is unambiguous only is the splitting is such that the averaged line falls on the real average of the positions of the unmerged lines. In the case of the ND_3 motion the idealized spectrum and the real spectrum differ markedly (see Fig. 20). The primary advantage of this type of measurement is that it may provide an estimate of the activation energy for a particular motion on the basis of a much less complex and expensive apparatus than is required for T_1 measurements.

DEUTERON SPIN-LATTICE RELAXATION.

The spin-lattice relaxation time T_1 for deuterons in LiDzS was measured by a double 90^o pulse technique. The

first pulse is applied to the system in equilibrium and the nuclear response a given time after the end of the pulse has a magnitude S_0. The second pulse is separated from the first pulse by a time t. The response S(t) to the second pulse was measured and fitted to the relation

$$S_0 - S(t) = S_0 e^{-t/T_1} . \qquad (3.14)$$

It can be shown* that for the three level deuteron system (m = -1, 0, +1), Eq. (3.14) holds only for the experiment carried out with the lines corresponding to transitions between m = (0↔+1) and m = (-1↔0) merged so that the population differences between the m = 0, m = 1 and m = 0, m = -1 levels are symmetrically reduced to zero. The equilibrium populations are then re-established with a single time constant, $T_1 = (P_1 + 2P_2)^{-1}$, where P_1 and P_2 are the probabilities for a $\Delta m = 1$ and $\Delta m = 2$ transition respectively.*

Fig. 23 shows the values of $1/T_1$ obtained by this method plotted against 1/T. Because of the complexity of the spectrum in the region below 0^oC it was not possible to carry out the experiment on the ND_3 lines at a crystal

*Appendix B contains a development of the equations pertinent to this section.

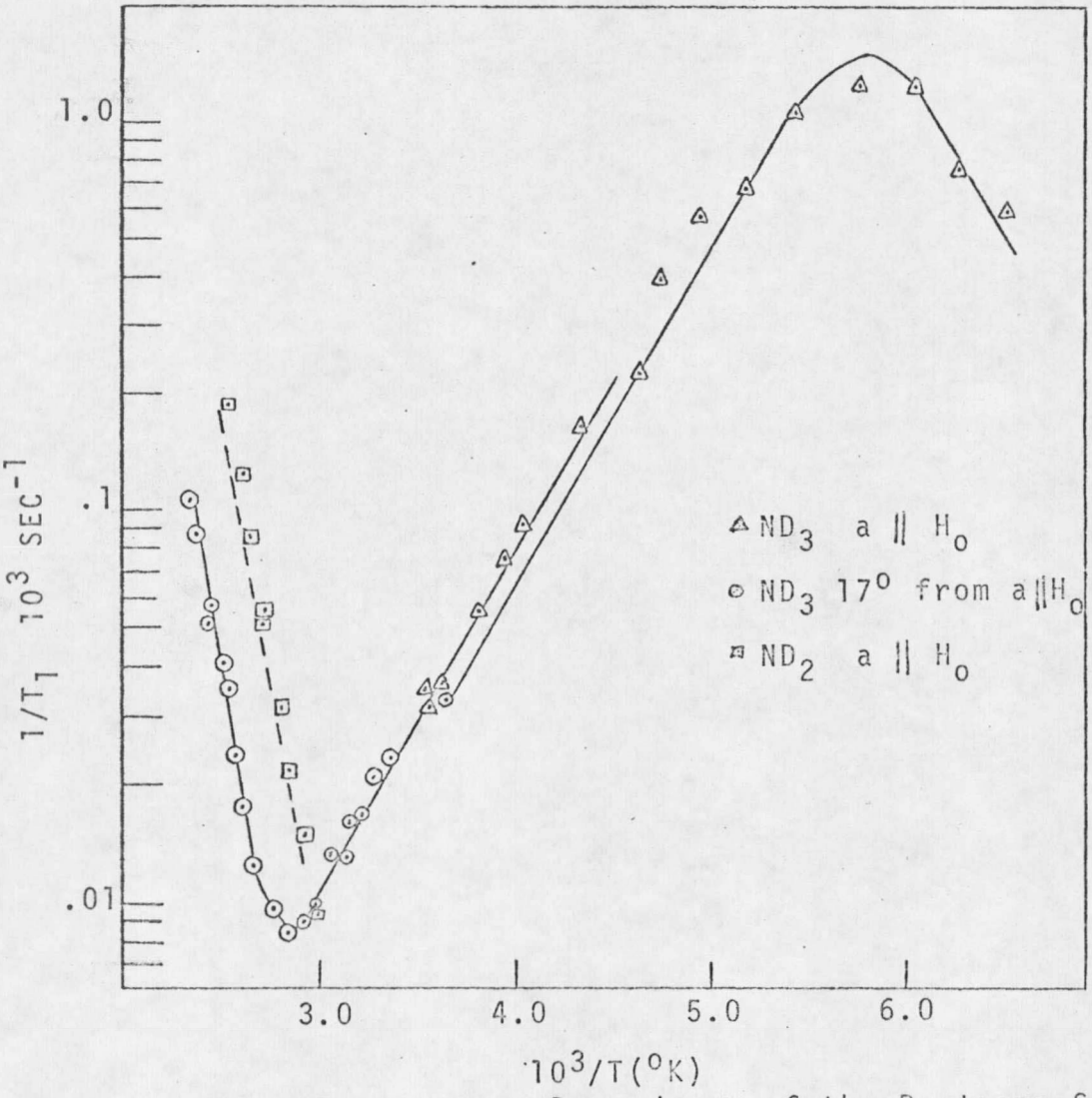


Fig. 23. Temperature Dependence of the Deuteron Spin-Lattice Relaxation Time.

orientation for which the line splitting was zero. Attempts to do so resulted in erroneous response, because the Fourier spectrum of the 90^{o} pulse contained components at the frequency of neighboring lines and consequently the response was modulated at a frequency determined by the separation between these lines. The same problem was encountered when measurements of T_1 for the ND_2 lines were attempted at the zero crossings. Consequently the ND_2 and low temperature ND_3 experiments were done with the crystal oriented with a $||H_o$.

The experimental results for a $||H_o$ and for the transition m = -1 to m = 0 appear to depend on only a single relaxation time which is taken to be the experimental T_1. The values of T_1 measured (Fig. 23) for the orientation a $||H_o$ were obtained by saturating the m = 0 to m = -1 transition and analyzing the response to determine this single relaxation time T_1. The theoretical response* for the experiment in which only one of the transitions is saturated is (3.15)

$$S_o - S(t) = \frac{1}{4} S_o \left[3 \exp(-3P_1)t + \exp -(P_1 + 2P_2)t\right] .$$

*Appendix B contains a development of the equations pertinent to this section.

TABLE VII

Values of Electric Field Gradient Tensor Components in the Crystal System Multiplied by K = 3eQ/2h, in kHz, for the Five Deuteron Sites in $LiN_2D_5SO_4$.

Site	$K\phi_{XX}$	$K\phi_{YY}$	$K\phi_{ZZ}$	$K\phi_{XY}$	$K\phi_{XZ}$	$K\phi_{YZ}$
1	-96.7	264.6	-167.9	-126.9	- 28.8	51.9
2	-71.2	-115.8	187.0	0.0	-152.3	-50.0
3	-99.3	221.8	-122.5	90.3	15.1	62.2
4	-58.0	-128.0	186.0	0.0	136.2	-17.7
5	50.0	- 96.5	46.0	75.7	-186.3	-84.3

TABLE VIII

Values of Electric Field Gradient Tensor Components in the System z' || a Multiplied by K = 3eQ/2h in kHz for the Five Deuteron Sites in $LiN_2H_5SO_4$.

Site	$K\phi_{x'x'}$	$K\phi_{y'y'}$	$K\phi_{z'z'}$	$K\phi_{x'y'}$	$K\phi_{x'z'}$	$K\phi_{y'z'}$
1	264.6	-167.9	- 96.7	51.9	-126.9	- 29.8
2	-115.8	187.0	- 71.2	- 50.0	0.0	-152.3
3	221.8	-122.5	- 99.3	62.2	90.3	15.1
4	-128.0	186.0	- 58	- 17.7	0.0	136.2
5	- 96.5	46.0	50.5	- 84.3	75.7	-186.3

TABLE IX

Values of the Electric Field Gradient Tensor Components in the System z' in the Plane of a,b and 18° from z' ∥ a Multiplied by K = 3eQ/2h in kHz for the Deuterons of Sites 3, 4, and 5 Separately. Also Included Are the D_3 Average efg Tensor Values (Same Orientation).

Site	$K\phi_{x'x'}$	$K\phi_{y'y'}$	$K\phi_{z'z'}$	$K\phi_{x'y'}$	$K\phi_{x'z'}$	$K\phi_{y'z'}$
3	-122.5	381.7	-259.2	- 54.5	33.6	- 94.4
4	186	-120.9	- 65.1	- 58.9	124.3	20.6
5	46.0	-126.8	80.8	- 22.7	-203.2	43.2
ND_3 (+72°)	36.7	28.5	- 65.2	- 16.3	7.0	10.7
ND_3 (-72°)	36.7	- 36.5	- 0.2	9.1	- 15.2	- 10.7

The values of the components of the field gradient tensors, ϕ_{ij}, were obtained by transforming from the tensor expressed relative to the crystal system by a rotation about the appropriate crystal axis through an angle θ to bring the z axis parallel to the field H_o. Table VII gives the components of the efg tensor in the crystal system for the bonds used in the analysis. The components of the efg tensor relative to a system in which z' $||$ a are given in Table VIII and the components of the efg tensor relative to a system in which the crystal is rotated about the c axis through the angle 72^o from z' $||$ b are given in Table IX.

The transition probabilities were calculated on the assumption that the exchange causing relaxation is associated with rotation of the ND_3 group or ND_2 group, as opposed to exchange between neighboring N_2D_5 groups. Using the values of P_1 and P_2 (see Table X) calculated for the a $||$ H_o data, values of $(S_o - S(t))$ can be plotted on semi-logarithmic paper against t. For values of $S_o - S(t) > 0.15$ these plots are almost linear which explains the fact that the experimental response seems to depend on a single relaxation time. By fitting a straight line to these plots a single effective relaxation time is found. This effective relaxation time T_{1e} is calculated for both the ND_2 and the ND_3 groups with a $||$ H_o. The relaxation time for the ND_3

TABLE X

Calculated Values of the $\Delta m = 1$ and $\Delta m = 2$ Transition Probabilities for the Cases of Interest

	P_1	P_2
$ND_3(H_o \parallel a)$		
$\omega T_c << 1$	$0.845 \times 10^{11} T_c/sec^2$	$2.02 \times 10^{11} T_c/sec^2$
$\omega T_c >> 1$	$\frac{0.845 \times 10^{11}}{\omega^2 T_c \ sec^2}$	$\frac{0.505 \times 10^{11}}{\omega^2 T_c \ sec^2}$
$ND_3(72^o$ from H_o b about c axis)		
$\omega T_c << 1$	$0.993 \times 10^{11} T_c/sec^2$	$1.48 \times 10^{11} T_c/sec^2$
$ND_2(H_o \parallel a)$		
$\omega T_c >> 1$	$0.152 \times 10^{11}/\omega^2 T_c sec^2$	$0.355 \times 10^{11}/\omega^2 T_c sec^2$

group with z' in the ab plane 72° from the b axis is obtained directly from $T_1 = (P_1 + 2P_2)^{-1}$. These calculated relaxation times all depend on τ_c, the correlation time. The frequency $\omega = 2\pi \times 14.020$ MHz was employed for the entire experiment. The assumption is made that $\tau_c = \tau_0 \exp(E_a/kT)$ so that the calculated relaxation times depend on the parameters E_a and τ_0.

In the temperature region below 250°K ($1/T > 4 \times 10^{-3}/°K$) a maximum in the $1/T_1$ curve is evident. The slopes of the curve in the regions above and below the peak are equal in magnitude, and depend through τ_c on the parameters E_a and τ_0. For temperature regions above and below the peak T_1 is proportional to $1/\tau_c$ and $\omega^2\tau_c$ respectively. The assumption is made that at the peak the high temperature T_1 must equal the low temperature T_1. This equation contains only the variables ω and τ_c. Since ω is known, the equation is solved for τ_c and it is found that $\tau_c = 1.02 \times 10^{-8}$ sec. By comparison the value obtained from the line width measurements at this temperature is $\tau_c = 4.3 \times 10^{-8}$ sec. The solid curve (Fig. 23) through this region is obtained by calculating $1/T_1 = \frac{5P_1 + P_2}{2}$ for τ_c in the region of 1.6×10^{-8} sec. This expression was obtained from the initial slope of the return to equilibrium of the population following a 90° pulse. The value of T_1 calculated from the

value of T_c at the intersection is $T_1 = 7.6 \times 10^{-4}$ sec. The best fit to the data gives an activation energy $E_a = 0.20 \pm 0.01$eV and $T_o = 1.6 \times 10^{-14}$ sec. The activation energy found by the line width technique is $E_a = 0.19$eV. By comparison $E_a = 0.182 \pm 0.013$eV for the NH_3 hindered rotation in $LiHzS$[12] and $T_o = 3 \times 10^{-14}$ sec for deuteron intrabond motion in KD_2PO_4.[7] A displacement in the best fit line occurs because of the difference in the values of T_1 depending on the orientation at which the measurement was made.

As the temperature increased, the value of $1/T_1$ for the ND_3 group begins to increase near $1/T = 2.80 \times 10^{-3}/^oK$. This must be explained by some different mechanism. Three explanations are considered. First, it is possible that there is reorientation of the entire N_2D_5 group. McClement, Pintar and Petch[13] suggest that such a motion might cause the large reduction in second moment and the frequency dependent relaxation times observed for $1/T \times 10^3/T(^oK)$ smaller than 3. However, the fact that the spectral lines due to the ND_3 average are still observed at 2.2 and do not appear broadened, implies a T_c for such a motion larger than 10^{-5} sec. This large value for T_c leads to impossibly large differences in field gradient values (of the order 10^2 or 10^3 larger than those measured) in order to achieve the short

relaxation times observed. Thus tumbling of the hydrazine groups is not the mechanism for relaxation.

Secondly, diffusion may take place between ND_3 groups. If such a motion is assumed the ND_3 average field gradient values for neighboring hydrazine groups (Table IX efg axes oriented at $\pm 72^{o}$) can be used to determine τ_c from the T_1 values measured in this temperature region. Using T_1 = 100 milliseconds which is the value observed at $1/T \simeq 2/3 \times 10^{-3}/^{o}K$ τ_c is calculated to be 1.6×10^{-9} sec. This value of τ_c corresponds to $\omega\tau_c << 1$. However, the slope of the $1/T_1$ versus $1/T$ curve observed in this region corresponds to $\omega\tau_c >> 1$ which makes diffusion between ND_3 groups an unacceptable explanation.

This leaves the possibility of jumping between ND_2 and ND_3 sites.

The T_1 measurements for the ND_2 group were carried out with the crystal oriented a $\| H_0$, making the relaxation behavior the same as that for the ND_3 group with a $\| H_0$. P_1 and P_2 are given in Table X and by best fitting Eq. (3.15) for these values of P_1 and P_2, the dependence of T_1 on τ_c is obtained. The T_1 values for the ND_2 group are 10 to 100 times shorter than those values predicted for the ND_3 relaxation time on the basis of jumping between ND_3 sites. It is reasonable that the jumping between ND_2 sites is the

primary relaxation mechanism for the deuterons of these sites. When a 90° pulse is applied to the ND_3 system, the ND_2 system stays approximately in equilibrium with the lattice since it has a much shorter T_1 than the ND_3 system. This means that the relaxation time measured for the ND_3 system is really a measure of the time for mixing between ND_2 and ND_3 populations.* Let this time be denoted T_m and assume that $T_m = T_{mo} e^{E_a/kT}$. The best fit for the ND_3 relaxation then gives $E_a = -.75 \pm 0.05$eV and an unusually long infinite temperature mixing time, $T_{mo} = 1.3 \times 10^{-11}$ sec.

The effect of the mixing on the relaxation of the ND_2 group cannot be neglected. When the ND_2 system is subjected to a 90° pulse, the contribution due to mixing is 3/2 the $1/T_1$ for the ND_3 site since it can be assumed that the ND_3 system stays nearly in equilibrium with the lattice during the short time that the ND_2 system relaxes. The factor 3/2 is introduced because the $1/T_1$ for the ND_3 is proportional to the fraction of the number of deuterons occupying ND_3 sites exchanging with deuterons of ND_2 sites. There are only 2/3 as many ND_2 sites as ND_3 sites so the jumping involves a fraction of the ND_2 sites 3/2 larger than the fraction of ND_3 sites. The $1/T_1$ for ND_2 sites, since it is proportional to

---

*See Appendix B for discussion of equations governing this exchange process.

the fraction of ND_2 sites jumping, must be proportional to 3/2 the $1/T_1$ for ND_3 sites. When this correction is made, the result is the dashed line in Fig. 23. The correlation time due to ND_2 hindered rotation has activation energy 0.50 ± 0.02eV and $\tau_o = 2.2 \times 10^{-14}$ sec. By comparison the activation energy obtained by means of the line width study is 0.46eV.

DISCUSSION.

The measurements described in this chapter clearly indicate certain motions of the deuterons in the crystal. The deuterons of the ND_3 group undergo a hindered rotation. This rotation provides the principal mechanism for the relaxation of these deuterons up to about 65°C. The correlation time for this motion as indicated from the line width study is ~ 10^{-4} sec at 100°K.

The deuterons of the ND_2 group exchange at a lower rate. On the basis of the line width measurements, a correlation time of 10^{-5} sec is predicted for this exchange near room temperature. The merged lines observed due to the average over the ND_2 sites appear near 50°C and the primary relaxation mechanism for these deuterons is provided by the exchange between ND_2 sites over the entire range studied, namely from T ≈ 50°C to T ≈ 110°C.

Measurement of the dielectric constant reveals two

contributions to the relaxation mechanism. The low temperature contribution has an activation energy ~0.40eV comparable to that for the D_2 exchange, while the high temperature contribution has an activation energy of about 0.70eV.

Jumping between the ND_2 and ND_3 sites explains the relaxation of ND_3 site deuterons from 65°C to the upper limit of the temperature range available with the apparatus. The activation energy for this mechanism is 0.75 ± 0.05eV which is slightly larger than the quoted c axis dc conductivity activation energy of 0.65eV. However, the activation energy for the high temperature contribution to the dielectric relaxation of 0.70eV is in good agreement.

The agreement between the activation energies for the very large c axis dielectric constants and those for the ND_2 exchange, and the ND_2 to ND_3 jumping indicates that the ND_2 motion may be associated with the mechanism responsible for the dielectric relaxation.

As is indicated in Fig. 1 there are n glides, b glides and twofold rotation axes in the crystal cell. Because of this symmetry of the crystal, reflection through the ab plane of a unit cell gives rise to a deuteron splitting spectrum identical to the spectrum observed for the unreflected cell. This coupled with the absence of any

positive indication in either the low temperature spectrum or the high temperature spectrum of a doubling of spectral lines is consistent with the idea that domain reversal takes place by way of reflection through the ab plane.

Although the deuteron spectrum above -85°C shows change which is possibly due to structural change in the crystal, no definite conclusions can be made as to the exact nature of the change. Certainly no indication of a ferroelectric transition is obtained below 190°C. This is in agreement with the absence of an anomaly in the dielectric constant below 200°C, which substantiates earlier claims[10] that no ferroelectric transition takes place below the decomposition temperature of the crystal.

CHAPTER IV EXPERIMENTAL

CRYSTAL PREPARATION.

Single crystals of $LiN_2H_5SO_4$ were prepared by dissolving stoichiometric amounts of Li_2CO_3 (reagent grade) and $(NH_2)_2 \cdot H_2SO_4$ (reagent grade) in water, and crystallizing by slow evaporation. Large (2.95cm x 3.05cm x 5.6cm, 34g.) single crystals with well developed (100), (110) and (101) faces can be grown by this technique. In order to obtain deuterated samples, the crystals of $LiN_2H_5SO_4$ obtained as described above were dissolved in 90% D_2O and recrystallized. An estimate of the percent of deuteration of these crystals was made by comparing proton signal strengths from two samples of equal size. The results indicated that the crystal was about 50% deuterated. A second recrystallization from 99% D_2O was then carried out. The crystallizing dish was placed in a desiccator during this process in order to minimize water vapor exchange with the atmosphere.

NMR SPECTRA.

A Robinson[32] circuit employing frequency modulation between 900 and 1500 Hz and operating at 14 MHz was used to obtain most of the NMR spectra. A solid state modification of this circuit[33] was used to obtain the room temperature data.

The permanent magnetic field for the experiment was

provided by a 15" Varian electromagnet with Model V-FR-2703 Fieldial control. The crystal was oriented relative to the permanent field H_0 by visually aligning it with a crystal axis parallel to the spectrometer tube. The spectrometer tube was fixed perpendicular to the circular spectrometer base plate, which was calibrated in degrees. The spectrometer then rested on its base in a circular holder in such a fashion that rotating the spectrometer in its holder rotated the tube and hence the crystal about the crystal axis perpendicular to the field. The rotation angle was read from the circular base plate.

The spectrum corresponding to a particular crystal orientation was typically obtained in the following fashion. The field dial was set so that the sweep center coincided with the center of the NMR spectrum and then the magnetic field was swept over the range including the spectrum. The sweep range varied from 50 gauss to 500 gauss depending on crystal orientation and temperature. Sweep times between 1 and 25 minutes were used.

The room temperature spectrum and part of the 77°K spectrum were obtained using a Princeton Applied Research (P.A.R.) Model JB-4 lock-in amplifier as the modulation source for the spectrometer, and signal detector and amplifier. All the remaining data was obtained using a

P.A.R. Model HR-8 lock-in amplifier. The output of the lock-in was ordinarily fed directly to either a Bristol time base chart recorder (Fig. 4 shows typical spectra) or a Moseley 7000 AR X-Y recorder (Fig. 16 shows typical spectra). The X drive for the X-Y plotter was provided by an output from the Fieldial magnet sweep control. The operating frequency of the spectrometer was monitored by a Hewlett Packard 5245L electronic counter with 5261A preamplifier.

Poor signal to noise ratio made necessary the employment of a signal averaging technique in order to obtain the spectra for certain orientations. The output of the lock-in detector was fed to a Vidar Model 240 voltage-to-frequency converter and the output of the converter was then stored in a Technical Measurement Corporation Model 401D 400 channel amplifier. The magnetic field sweep was coordinated with the storage rate of the multichannel analyzer. The accumulated storage of from 3 to 10 sweeps was then called out of the multi-channel analyzer and recorded in a form suitable for analysis. A block diagram of the experiment is shown in Fig. 24.

Temperatures for this experiment were held within $\pm 5^{o}C$ for obtaining spectra, and within $\pm 1^{o}C$ for the line width study. The $77^{o}K$ spectrum was obtained by submerging, in a

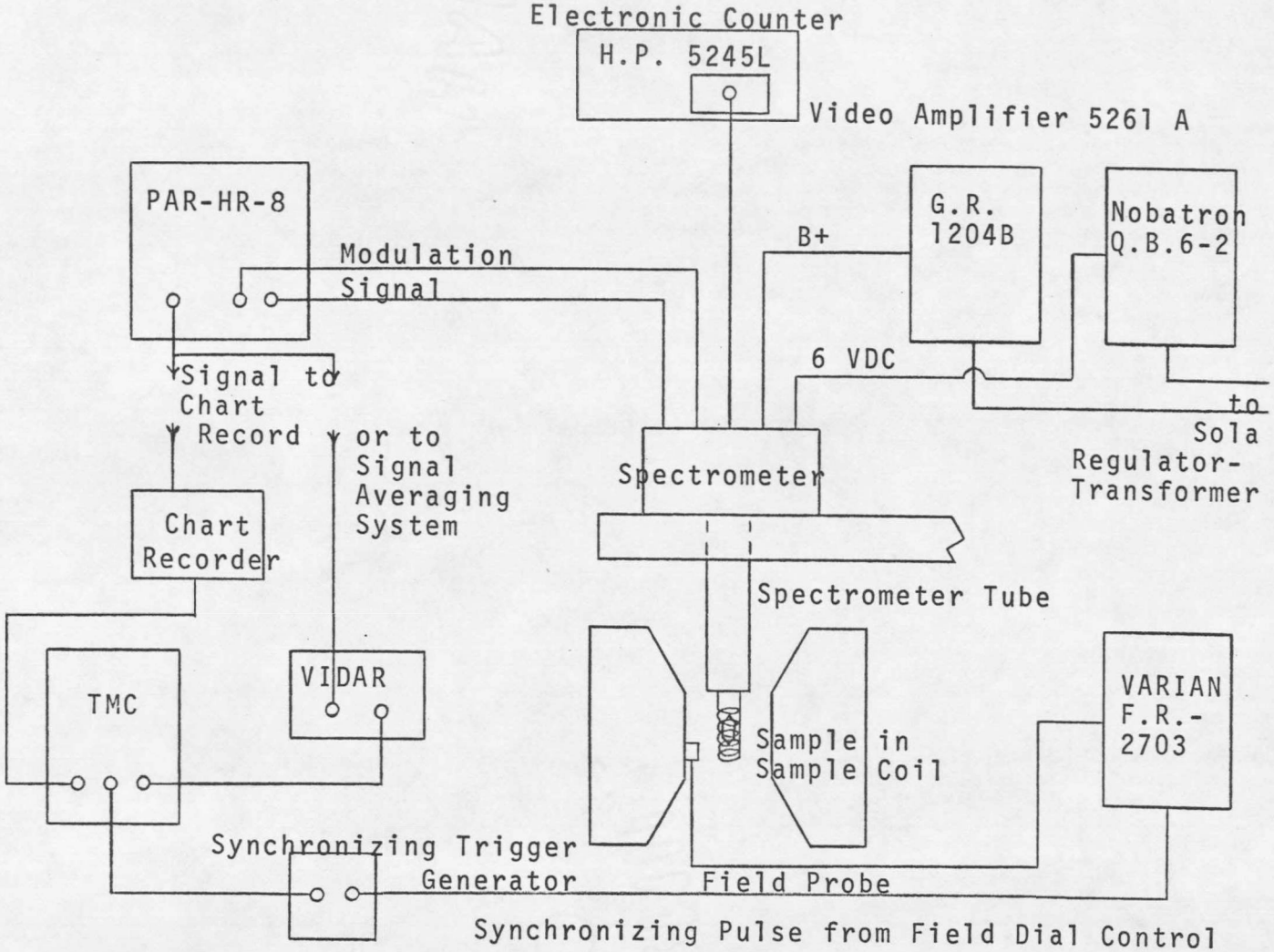


Fig. 24. Block Diagram of NMR Spectrometer.

Dewar of liquid air, the sample and sample coil which were sealed in a brass can. The temperature at the boiling point of liquid air at Bozeman is 77.3°K. The 193°K spectrum was obtained by submerging the sample sealed in a brass can in a Dewar of methanol. The temperature of the methanol was controlled by the addition of liquid air. A chromel-alumel thermocouple was used to measure the temperature of the bath. Some of the measurements taken at 65° and 95°C were obtained using as a bath silicone oil heated with a resistor. The line broadening of the ND_2 group was studied in this same fashion. The remainder of the measurements at elevated temperature were made by means of an electric heater in good thermal contact with a brass can surrounding the sample.* A stainless steel insulating tube was placed around the heating coil, thermal connector and sample to provide thermal isolation for the system. The temperature control employed to obtain ±1° tolerance for the line broadening data at low temperature was effected by means of a spectrometer tube built as an integral part of a liquid air reservoir.* The neck separating the sample coil from the reservoir was wound with a heating element and control is exercised by means of

*The two temperature control devices are pictured in detail in reference 34.

the current passed through the heating element.

CONDUCTIVITY AND DIELECTRIC CONSTANT.

Samples suitable for both conductivity and dielectric constant measurements were obtained by cutting small wafer shaped sections from large single crystals with a string saw. Care was taken to guarantee that the normals to the large surfaces or faces of these wafers were parallel to a crystal axis. These faces were then polished with a damp paper and contacts were painted on them. One contact was a round dot with average area of $4 \times 10^{-2} cm^2$. A guard ring was then painted around the circular contact. The average thickness for the samples was about 0.15 cm.

A block diagram of the conductivity experiment is shown in Fig. 25. The conductivity is

$$\sigma = \frac{1}{\rho} = \frac{t}{A} \times \frac{1}{R_c} ,$$

where t = crystal thickness, A is the area of the circular contact, and R_c is the resistance of the crystal. (The crystal equivalent circuit is shown in Fig. 26). The current through the crystal is the sum of the current through R_c and R_s. R_g represents the resistance through the crystal to the guard ring, including the surface between the ring and the contact on the opposite crystal

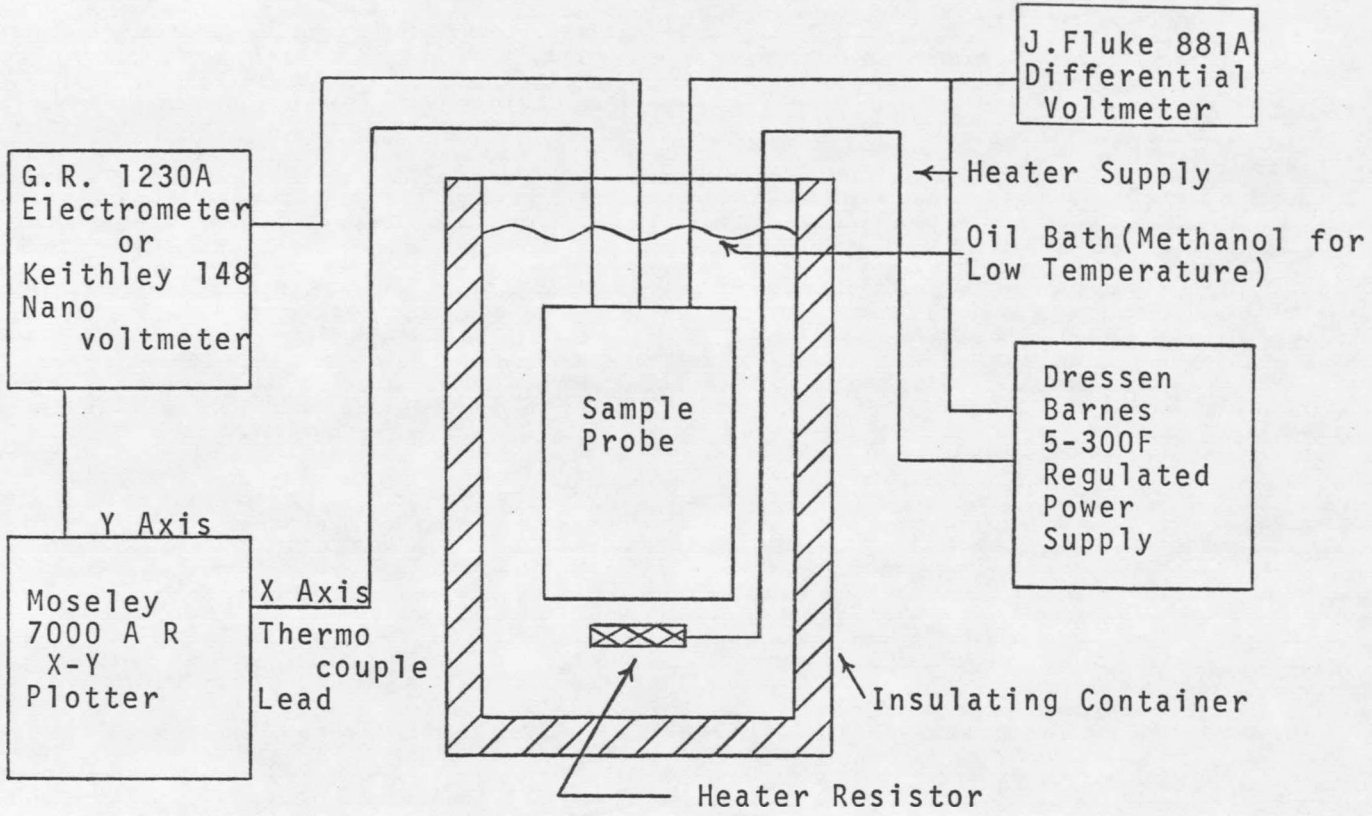


Fig. 25. Block Diagram of Conductivity Experiment

face. R_s is the resistance between guard ring and the center contact on the same face, and R_c is the crystal resistance.

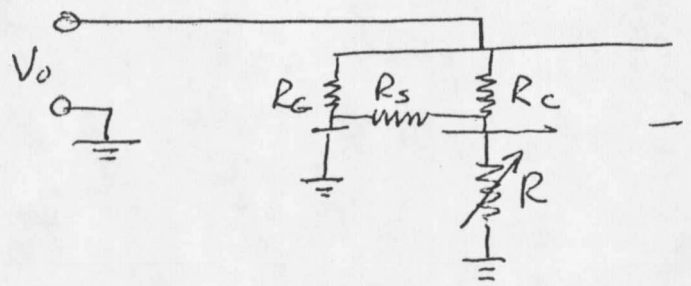


Fig. 26. Crystal Equivalent Circuit

If R is made small compared to R_c and R_s, then the current through R_s is negligible compared to that through R_c, so the current through the electrometer resistance R is approximately the current through R_c and since $IR << IR_c$ the voltage V_o is dropped almost entirely across R_c. Thus $R_c = \frac{V_o}{I}$ to a good approximation, where V_o is the applied voltage and I is the current measured through the electrometer. For voltages between 10 and 300 volts a Dressen Barnes 5-300F regulated power supply was used to supply V_o. The voltage was measured with a J. Fluke Model

881 differential voltmeter. Below 10 volts the differential voltmeter was used as the source of V_o. Typical values for the crystal resistance range between 10^7 and 10^{15} ohms for the assortment of samples and temperatures studied. Electrometer resistance was held at least 100 times smaller than R_c. In order to accomplish this, a General Radio Model 1230A electrometer was used as a Keithley Model 148 nanovoltmeter.

Elevated temperatures were obtained by placing the sample probe within a leak-proof container and submerging the assembly in a bath of mineral oil. The bath temperature was controlled by controlling the current through a resistor in the bath. Lower temperatures were obtained by using methanol as a bath and adding liquid air in small amounts. The temperature was measured with a chromel-alumel thermocouple, which was used to provide the x axis drive voltage for the Moseley 7000 AR X-Y plotter. The output of the electrometer was fed into the y axis input of the plotter. This allowed a continuous measurement of the crystal current vs temperature. The voltage applied to the sample was reversed periodically in order to minimize build-up of high resistance layers adjacent to the electrodes (electrode "polarization"). Upon reversing the voltage,

large transient current was observed. The average current indicated after the decay of the transient was taken to be representative of the crystal conductivity.

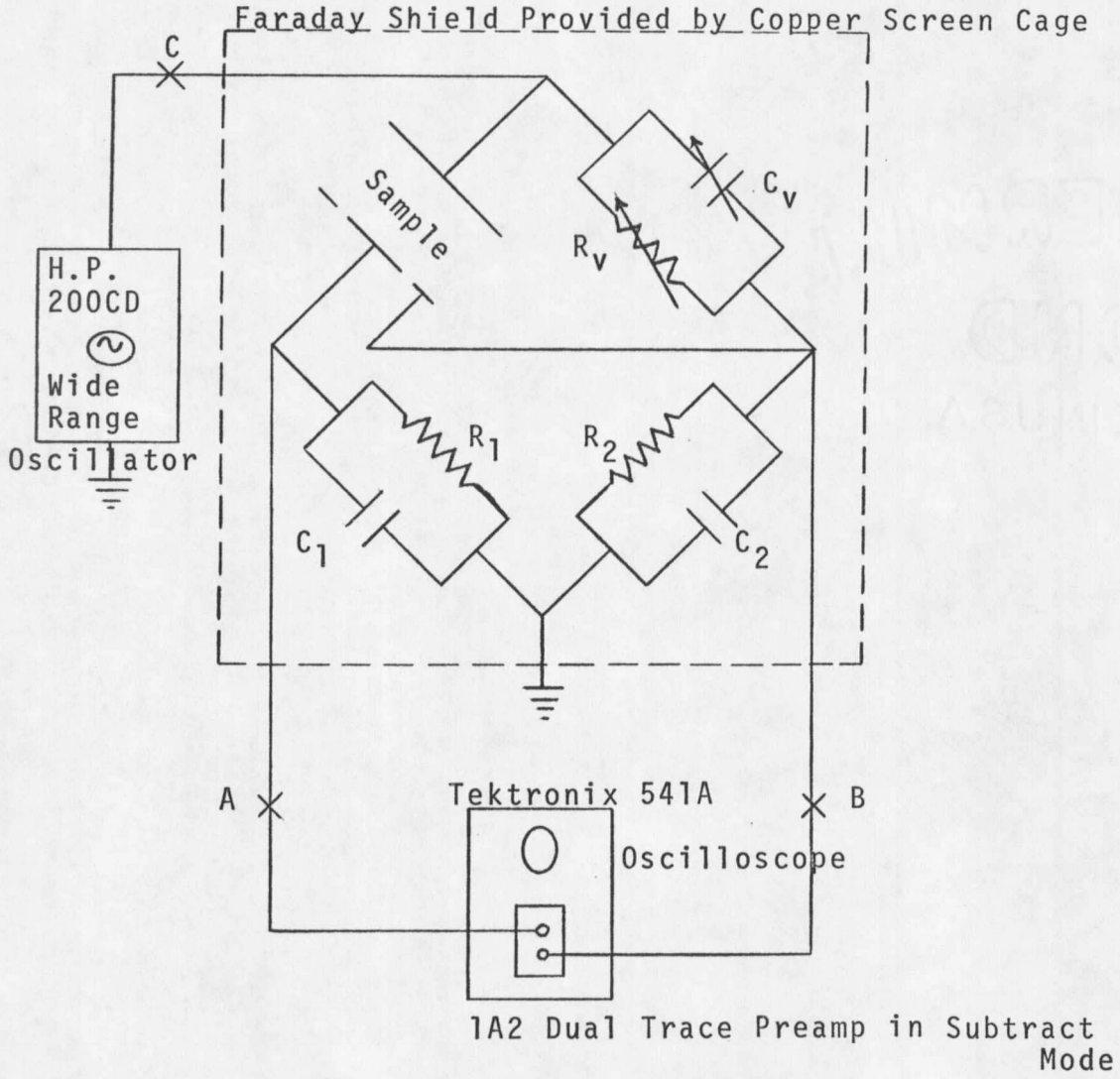
The ac dielectric constant was measured with a bridge circuit. A diagram of the circuit is shown in Fig. 27. The crystal holder is pictured in Fig. 28.* A Tektronix 541A oscilloscope with a Type 1A2 dual preamp in the subtract mode, which provides for superposition of the signals in the two channels of the preamp, was used to detect the balanced bride condition. For measurements of the a axis dielectric constant the P.A.R. Model HR8 lock-in detector with the preamplifier in the difference mode was used. With the bridge balanced the capacitance and resistance of the sample are in the same ratios to C_v and R_v as C_1 and R_1 are to C_2 and R_2. The following equations are then used to calculate the real and imaginary parts of the dielectric constant $\varepsilon = \varepsilon' - i\varepsilon''$:

$$\varepsilon' = \frac{tC_c}{\varepsilon_o A} \qquad \varepsilon'' = \frac{t}{\varepsilon_o \omega A R_c}$$

Here C_c, R_c, and t are the sample capacitance, resistance and thickness respectively, A is the area of contact, and

---

*The crystal holder was designed and constructed by Prof. V. H. Schmidt.



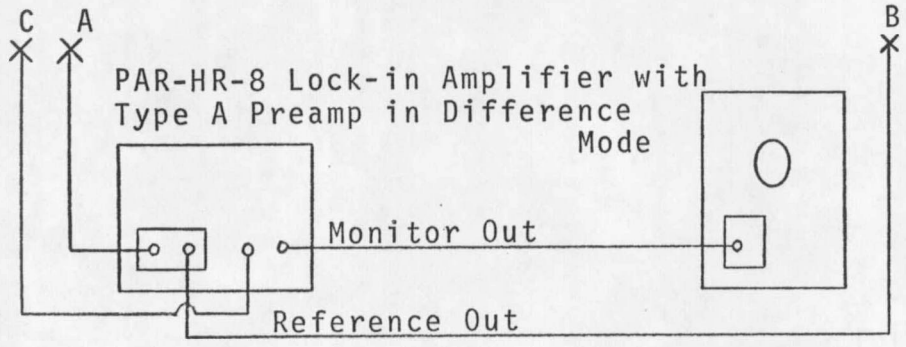


Fig. 27. Diagram of Dielectric Constant Measurement Circuit.

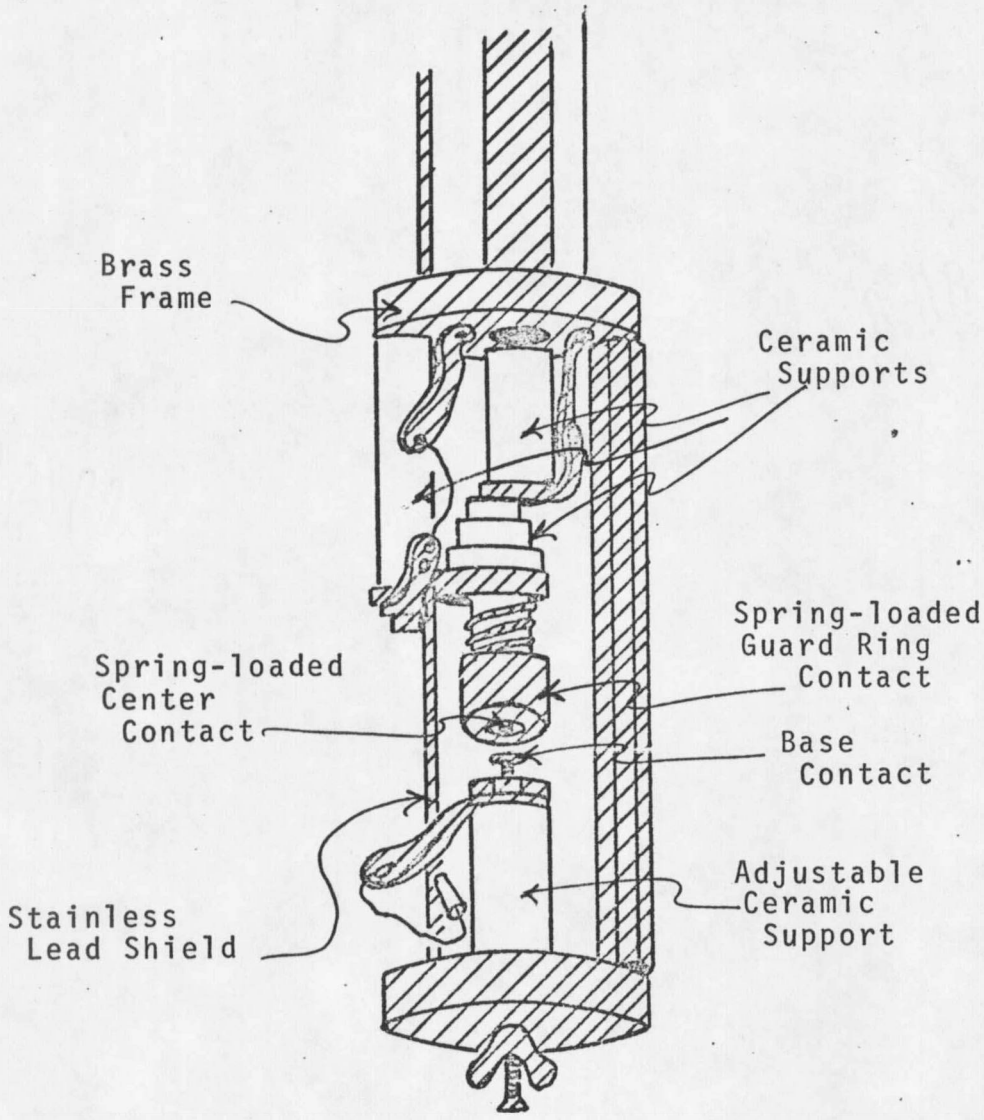


Fig. 28. Sample Probe Employed for the Dielectric Constant Measurement.

ω the angular frequency of the ac voltage at which the measurement is made.

The temperature of the crystal was controlled by placing the sample holder in its protective brass container in a bath of fine sand. Temperatures above room temperature were obtained by passing a current through a resistor buried in the sand bath. To lower the temperature, the bath was cooled by adding small quantities of liquid air. The temperature was measured with a chromel-alumel thermocouple.

RELAXATION TIME.

The spin-lattice relaxation time measurements were made with a double 90^{o} pulse sequence. The initial trigger was supplied by a pulse generator supplying single pulses at 1.3 sec to 5 min intervals. The trigger was fed to a Tektronix Type 162 waveform generator, which produces a sawtooth of variable length as well as a pulse. The pulse and sawtooth were fed separately to two Tektronix Model 163 pulse generators to allow the 163 triggered by the sawtooth to fire at a time after the 163 triggered from the pulse. This time was controlled by changing the point along the sawtooth at which the voltage had risen to a value sufficient to trigger the pulse generator. Pulse lengths and separation were measured with a Hewlett Packard 5245-L

electronic counter with 5262A time interval unit and an H.P. 5321A time interval unit. The outputs from the pulse generators were fed to a pulse amplifier and then to an rf gating circuit which derives rf input from a crystal controlled 14.020 MHz oscillator. The output of the rf gate drives an rf pulse transmitter.* The output of the pulse transmitter is fed to a crossed coil pulse head.(34) The nuclear decay signal is picked up in the sample holder and fed to a preamplifier and then to a pulse receiver. The signal output of the receiver was measured with a boxcar integrator, the output of which is measured by a Minneapolis Honeywell potentiometer, Model 2730. A block diagram of the apparatus is pictured in Fig. 29.

A typical measurement is obtained by subjecting the sample to two 90^{o} pulses separated by a time t. The nuclear signal is measured during the tail following the second pulse by feeding the output of the pulse receiver during a brief period of the tail into the boxcar integrator. By repeating this procedure for many pulse sequences, noise is averaged and the output of the boxcar is measured with the potentiometer. The time t separating

---

*The pulse apparatus was constructed by Robert Parker and Fred J. Blankenburg. The basic design is after Clark et al.(35,36)

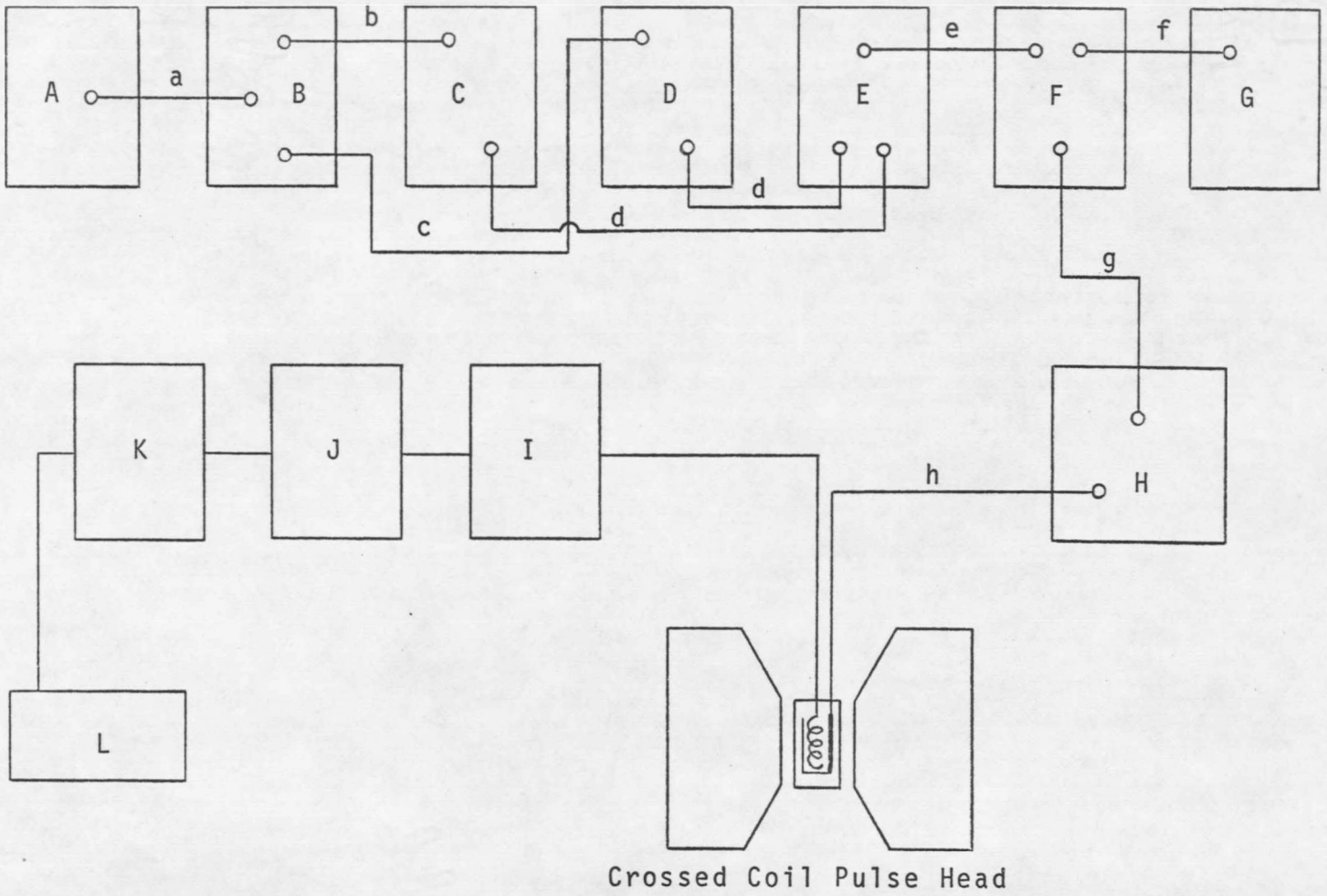


Fig. 29. Block Diagram of Pulse Apparatus

A - Trigger Pulse Generator

B - Tektronix Model 162 Waveform Generator

C - Tektronix Model 163 Pulse Generator

D - Tektronix Model 163 Pulse Generator

E - Pulse Amplifier

F - Radio Frequency Gate

G - Crystal Controlled Oscillator

H - Radio Frequency Pulse Transmitter

I - Radio Frequency Preamplifier

J - Pulse Amplifier

K - Box Car Integrator

L - Potentiometer

a -

b -

c -

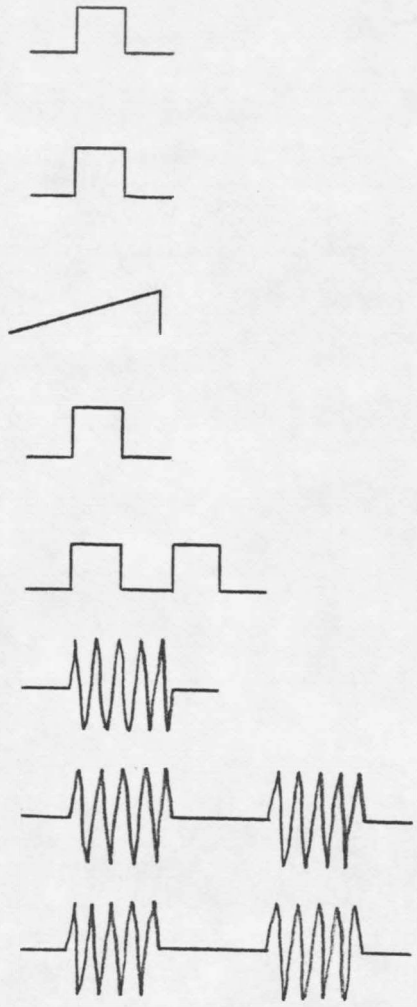
d -

e -

f -

g -

h -



Key for Fig. 29

the two pulses is changed and the entire procedure is repeated. The slope of a semilog plot of signal voltage versus t makes possible the calculation of the spin-lattice relaxation time T_1.

Temperature control is achieved by passing hot or cold air into the pulse head in such a fashion that the air is directed uniformly over the crystal. Cold air is provided by boil-off from a container of liquid air. Heated air is obtained by passing air from the Physics Building compressed air system through a regulator, then through a tube containing an electric heating element and finally into a pulse head. The temperature was measured with a chromel-alumel thermocouple attached to the crystal. Temperature variation for the measurements above room temperature was $\pm 1^{o}C$ and below room temperature $\pm 1.5^{o}C$.

APPENDIX A

Nuclei of spin $I \geq 1$ may possess an electric quadrupole moment.* If such a nucleus is placed at a site of non-vanishing electric field gradient (efg), and interaction between the nuclear quadrupole moment and the efg may be observed. The Hamiltonian of such an interaction, H_Q, is given by the tensor product of the nuclear quadrupole moment tensor with the efg tensor. Transitions between the energy states of the system can be induced by coupling the magnetic component of a resonant radio frequency field ($E = h\nu$) with the magnetic moment of the nucleus. In this fashion it is possible to measure the interaction energy characterized by H_Q.

Three important cases are distinguished with regard to this problem. The first case, that termed pure nuclear quadrupole resonance, is outlined above. The second case, called the weak field or Zeeman case, consists of subjecting the system of nuclei at sites of nonzero efg, to a weak permanent magnetic field H_o (~10 gauss). The Hamiltonian for the system is then $H_{tot} = H_Q + H_{mag}$, where the magnetic interaction is treated as a perturbation on the quadrupolar interaction energy. The third case consists of subjecting

---

*General discussion of the topic of this appendix is found in references 37 and 38.

a system of nuclei wherein the quadrupolar interaction is relatively small, to a strong magnetic field ($\sim 10^4$ gauss). The Hamiltonian is then $H_{tot} = H_{mag} + H_Q$ with H_Q the perturbation.*

In the present work the problem was the determination of the efg tensor at the hydrogen sites. In order to do this, deuterons ($Q = 2.77 \times 10^{-24}$ cm^2) were substituted for protons ($Q=0$). The experiment falls in the category of case 3. The calculation of the energies proceeds by choosing a representation in which I^2 and I_z are simultaneously diagonal. The basis states are denoted, $|I,m,n)$, where

$$I^2|I,m,n) = I(I+1)|I,m,n)$$

$$I_z|I,m,n) = m|I,m,n) \ .$$

The energy to zeroth order is the magnetic interaction energy

$$E_0 = (I,m| \underbrace{-\gamma H_0 I_z}_{\gamma H_0 m}|I,m) \qquad (A.1)$$

where H_0 is the permanent magnetic field directed along the z axis, γ is the gyromagnetic ratio, I_z is the z component of the nuclear angular momentum operator, and m is the magnetic quantum number. The perturbation is

---

*This case is considered by Volkoff[39] and the experiment is described in detail in the work of Volkoff, Petch and Smellie.[40]

$$H_Q = \frac{eQ}{2I(2I-1)} \left\{ (3I_z^2 - I^2)(\nabla E)_0 + \frac{\sqrt{6}}{2}(I_z I_+ + I_+ I_z)(\nabla E)_{-1} \right.$$
$$\left. + \frac{\sqrt{6}}{2}(I_z I_- + I_- I_z)(\nabla E)_{+1} + \frac{\sqrt{6}}{2} I_+^2 (\nabla E)_{-2} + \frac{\sqrt{6}}{2} I_-^2 (\nabla E)_{+2} \right\}. \quad (A.2)$$

e is the electron charge, Q the nuclear quadrupole moment and I is the nuclear angular momentum. The raising and lowering operators are defined $I_\pm = (I_x \pm iI_y)$ and the components of the efg tensor (with the z axis established by the magnetic field H_o) are given by

$$\nabla E_o = \frac{1}{2} \phi_{zz} \quad (A.3)$$

$$(\nabla E)_{\pm 1} = \pm \frac{1}{\sqrt{6}} (\phi_{zx} \pm i\phi_{yz}) \quad (A.4)$$

$$(\nabla E)_{\pm 2} = \frac{1}{2\sqrt{6}} (\phi_{xx} - \phi_{yy} \pm 2i\phi_{xy}) \quad . \quad (A.5)$$

The first order correction is

$$E_1 = \frac{eQ}{2I(2I-1)} \left[3m^2 - I(I+1) \right] (\nabla E)_o \quad . \quad (A.6)$$

The second order correction is

$$E_2 = \left(\frac{eQ}{2I(2I-1)} \right)^2 \left[\frac{3}{g\beta H_o} \left(m \left[4I(I+1) - 1 - 8m^2 \right] \right) |(\nabla E)_{\pm 1}|^2 \right.$$
$$\left. - \frac{3}{g\beta H_o} \left(m \left[2I(I+1) - 2m^2 - 1 \right] \right) |(\nabla E)_{\pm 2}|^2 \right] . \quad (A.7)$$

In general $|\nabla E_\mu|^2 (\mu = \pm 1, 2)$ can be expressed in units of $eq = \phi_{z'z'}$* relative to $z \parallel H_0$ with x, y arbitrary. Then

$$|\nabla E_\mu|^2 = e^2 q^2 |\nabla \hat{E}_\mu|^2 \tag{A.8}$$

and setting $\frac{e^2qQ}{h} = K$(coupling constant) and $g\beta H_0 = h\nu_L$ (ν_L, the Larmor frequency of the nucleus)

$$E_1 = \frac{hK}{2I(2I-1)} \left[3m^2 - I(I+1)\right] (\nabla \hat{E})_0 \tag{A.9}$$

and $$E_2 = \frac{3h}{2I(2I-1)^2} \frac{K^2}{\nu_L} \left[3\left(m\left[4I(I+1) - 1 - 8m^2\right]\right) |(\nabla \hat{E})_{\pm 1}|^2 \right.$$

$$\left. - 3\left(m\left[2I(I+1) - 2m^2 - 1\right]\right) |(\nabla \hat{E})_{\pm 2}|^2 \right]. \tag{A.10}$$

It can be seen that K/ν_L measures the magnitude of E_2 relative to E_1. The maximum value for the coupling constant is about 200 kHz. The Larmor frequency is 14 MHz. This makes $\frac{K}{\nu_L} = \frac{2 \times 10^5}{1.4 \times 10^7}$ and E_2 down some two orders of magnitude from first order effects. The shift in the center of the pattern resulting from the second order effect would then be of the same magnitude as the line widths observed. This is about the same size as the estimated error in the experiment, hence the second order effect is not studied. It can be seen that the first order correction depends on

---

*z' denotes the axis of the largest component of the efg tensor expressed in diagonal form.

the nuclear spin I, the nuclear quadrupole moment Q, and the quantity $(\nabla E)_o = \frac{1}{2}\phi_{zz}$ where ϕ_{zz} is the second derivative of the electrostatic potential at the nuclear site, with z parallel to H_o.

For deuterons the energy is given by

$$E = -\gamma H_o m + \frac{eQ}{2}(3m^2 - 2)\frac{\phi_{zz}}{2} \qquad (A.11)$$

The magnetic levels of the deuteron are shifted by the quadrupole interaction, causing the single absorption line at γH_o to split into two lines spaced equally on both sides of the unperturbed line, as pictured in Fig. 30. These lines are separated by a frequency $3\ eQ/h(\nabla E_o)$.

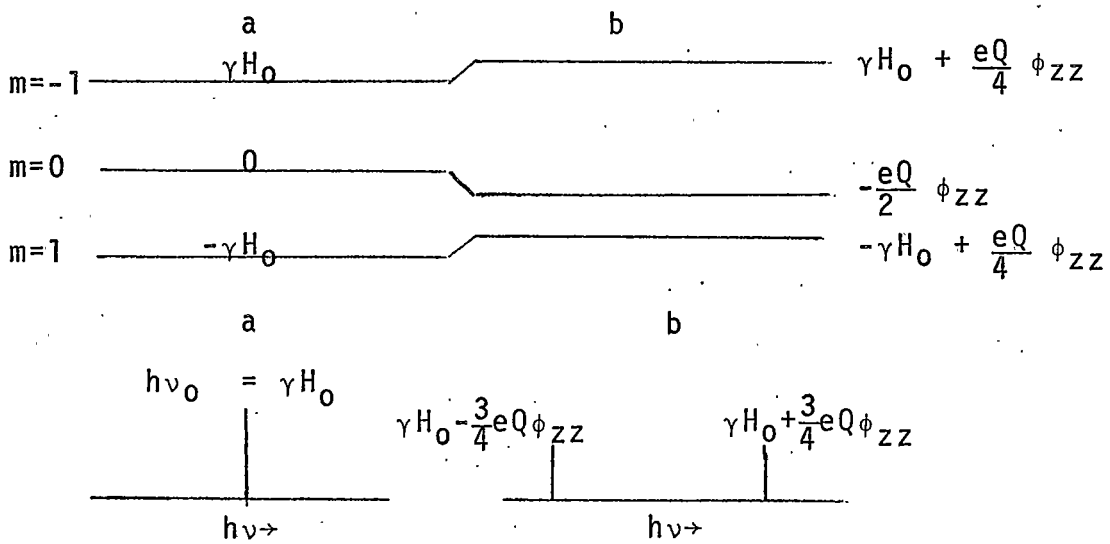


Fig. 30. a) Zeeman Levels and Transition Frequency b) Zeeman Levels Shifted by 1st Order Quadrupole Perturbation and Corresponding Transition Frequencies.

Changing the orientation of the sample relative to the constant field H_0, changes the component of the efg tensor along H_0. The result is that the splitting observed between the spectral lines changes. Because the efg tensor is symmetric ($\nabla \times E = 0$) and traceless ($\nabla \cdot E = 0$) it has only five independent components. The tensor can be put into the form

$$\phi_{ij} = \begin{pmatrix} -eq(1-\eta)/2 & 0 & 0 \\ 0 & -eq(1+\eta)/2 & 0 \\ 0 & 0 & eq \end{pmatrix} \qquad (A.12)$$

where eq is the largest and $-eq(1-\eta)/2$ the smallest component, making $|(\phi_{x'x'} - \phi_{y'y'})\ \phi_{z'z'}| = \eta$ lie in the range $0 \leq \eta \leq 1$. The values of η, eq, and three independent direction cosines specifying the orientation of the diagonal tensor relative to the crystal axes constitute five independent quantities.

A transformation can be carried out between the crystal and laboratory systems which relates the efg tensor to the system fixed in the crystal, through Eq. (2.1). The A, B and C of Eq. (2.1) are related to the components of the efg tensor in the crystal system as follows:

$$A_i = \frac{3eQ}{2h}(\phi_{jj} + \phi_{kk}) = -\frac{3eQ}{2h}\phi_{ii} \qquad (A.13)$$

$$B_i = \frac{3eQ}{2h}(\phi_{jj} - \phi_{kk}) \qquad (A.14)$$

$$C_i = -\frac{3eQ}{2h}\, jk;\ i,j,k = x,y,z \qquad (A.15)$$

As was discussed in Chapter I, the experimental curves of splitting frequency versus angle for rotation about the three crystal axes determine values for the A, B and C from which are found the components of the efg tensor in the crystal system. This tensor is then diagonalized and the values of the coupling constant, asymmetry parameter and the orientation of the efg tensor principal axis system in the crystal are obtained.

APPENDIX B

The deuteron system is a three level system so that relaxation processes may take place by way of $\Delta m = 1 (P_1)$ or $\Delta m = 2 (P_2)$ transitions. In order to calculate the probability of a transition between levels of the system, it is assumed that the mechanism responsible for the transition is the fluctuation in the nuclear quadrupole interaction due to deuteron jumping between sites of different electric field gradient. The calculation proceeds[9] by taking as the probability per unit time of a transition between states k and m

$$P_{mk} = \frac{1}{\pi^2} \int_{-\infty}^{\infty} G_{mk}(\tau) e^{-i(m-k)\tau} d\tau \qquad (B.1)$$

where the correlation function is defined

$$G_{mk}(\tau) = \overline{(m|H_Q(t)|k)(k|H_Q(t+\tau)|m)} \qquad (B.2)$$

the bar denoting an ensemble average over all values of $(m|H_Q(t)|k)$. The value of $G_{mk}(\tau)$ must be determined for two cases, exchange between two sites (ND_2 group) and exchange among three sites (ND_3 group). Having determined the values for $G_{mk}(\tau)$ for these two cases, it is then possible to calculate P_{mk} for the two cases. The relaxation times are then calculated from a knowledge of the population distributions immediately following a 90^0 pulse. Substitution of the values for P_1 and P_2 calculated

above yield expressions for the relaxation times depending only on the correlation time τ_c, and the Larmor frequency of the nucleus.

Consider first the calculation of G_{mk} for the case of jumping between two sites. Denote the sites as site 1 and site 2 corresponding to the deuteron positions indicated in Chapter II. Let $\hbar m = E_m$ and $\hbar k = E_k$ so that $(m - k) = (\frac{E_m - E_k}{\hbar}) = \omega$. Assume that exchange takes place as follows. Let there be n nuclei equally distributed between sites 1 and 2, and consider nuclei that at $\tau = 0$ a) occupy site 1 or b) occupy site 2. The element of the ensemble average corresponding to a is then $\frac{F_1}{2}\left[P_1(\tau)F_1 + P_2(\tau)F_2\right]$ where $F_1(i = 1,2)$ denotes that part of the Hamiltonian representative of the environment of site 1 which differs from site 2, so that as the nuclei exchange from site 1 to site 2 the interaction energy changes. For the case under consideration, F_1 represents the factor in the matrix element of H_Q containing the efg components. $P_i(\tau)$ is the probability that at time τ, the nucleus will be found at site 1. The remaining element of the ensemble average is

$$\frac{F_2}{2}\left[P_1(\tau)F_1 + P_2(\tau)F_2\right]$$

corresponding to b. Then (B.3)

$$\overline{F(o)F(T)} = \frac{F_1}{2}\left[P_1(T)F_1 + P_2(T)F_2\right] + \frac{F_2}{2}\left[P_1(T)F_1 + P_2(T)F_2\right] .$$

To determine $P_1(T)$ and $P_2(T)$, choose an ensemble with n_1 nuclei in site 1 and n_2 nuclei in site 2. Let $n_1 + n_2 = n$ and denote the probability of rotation through $+180^o$ between sites 1 and 2, P_{r+} so that $P_{r+} = P_{r-} = \frac{P_r}{2}$, P_r being probability of exchange due to + or - 180^o rotation. The equations describing the populations are, denoting $\frac{d}{dt}$ by $\cdot$,

$$\dot{n}_1 = -P_r n_1 + P_r n_2 = -\dot{n}_2 \qquad (B.4)$$

$$\dot{n}_2 = -P_r n_2 + P_r n_1$$

which are satisfied by $n_1 = \frac{n}{2} + \frac{n}{2}e^{-2P_rT}$ and

$n_2 = +\frac{n}{2} - \frac{n}{2}e^{-2P_rT}$; then $P_1(T) = \frac{n_1}{n} = \frac{1}{2}(1+e^{-2P_rT})$ and

$P_2(T) = \frac{n_2}{n} = \frac{1}{2}(1-e^{-2P_rT})$ making

$$\begin{aligned}\overline{F(o)F(T)} &= \frac{F_1}{2}\left[\frac{1}{2}(1+e^{-2P_rT})F_1 + \frac{1}{2}(1-e^{-2P_rT})F_2\right] \\ &\quad + \frac{F_2}{2}\left[\frac{1}{2}(1-e^{-2P_rT})F_1 + \frac{1}{2}(1+e^{-2P_rT})F_2\right] \\ &= \text{constant} + \frac{F_1}{4}\left[e^{-2P_rT}F_1 - e^{-2P_rT}F_2\right] \\ &\quad + \frac{F_2}{4}\left[-e^{-2P_rT}F_1 + e^{-2P_rT}F_2\right] . \qquad (B.5)\end{aligned}$$

The constant term does not contribute to the relaxation and is dropped. This leaves

$$\overline{F(o)F(\tau)} = \frac{1}{4}(F_1 - F_2)^2 e^{-\tau/\tau_c} \quad , \text{ where } 2P_r = 1/\tau_c \, .$$

Then for the $\Delta m = 1$ transition,

$$G_{\Delta 1}(\tau) = \left| \frac{eQ}{4I(2I-1)} (2m \pm 1) \left[(I \pm m)(I \pm m + 1) \right]^{\frac{1}{2}} \right|^2 \frac{1}{4}(F_1 - F_2)^2 e^{-\tau/\tau_c} \quad . \quad (B.6)$$

Here $F_i = \frac{1}{2}(\phi_{xx_i} - \phi_{yy_i}) \pm i\phi_{xy_i}$, $(i = 1,2)$ denoting sites 1 or 2. Specializing to $I = 1$ makes

$$G_{\Delta 1}(\tau) = \frac{e^2Q^2}{32}(F_1 - F_2)^2 e^{-\tau/\tau_c} \quad (B.7)$$

and

$$P_1 = \frac{4\pi^2}{h^2} \int_{-\infty}^{\infty} \frac{e^2Q^2}{32}(F_1^2 - F_2^2)\, e^{-\tau/\tau_c - i\omega\tau} d\tau$$

$$= \frac{\pi^2 e^2 Q^2}{4h^2} \left[(\Delta\phi_{xz})^2 + (\Delta\phi_{yz})^2 \right] \frac{\tau_c}{1+\omega^2\tau_c^2} \quad (B.8)$$

where $\Delta\phi_{ij}$ means ϕ_{ij}(site 2)$-\phi_{ij}$(site 1). For the $\Delta m = 2$ transition

$$G_{\Delta 2}(\tau) = \frac{e^2Q^2}{4}(F_1 - F_2)^2 e^{-\tau/\tau_c} \quad (B.9)$$

which gives for the transition probability

$$P_2 = \frac{4\pi^2}{h^2} \int_{-\infty}^{\infty} \frac{e^2Q^2}{4} (F_1^2 - F_2^2) e^{-\tau/\tau_c - i2\omega\tau} d\tau \quad . \quad (B.10)$$

$$= \frac{\pi^2 e^2 Q^2}{8h^2}\left[\Delta(\phi_{xx} - \phi_{yy})^2 + 4(\Delta\phi_{xy})^2\right]\frac{T_c}{1+4\omega^2 T_c^2} \quad . \quad (B.11)$$

The same arguments are then applied to the case of jumping among sites 1, 2 and 3. Transition probabilities obtained for exchange among the sites 1, 2 and 3 are

$$P_1 = \frac{\pi^2 e^2 Q^2}{9h^2}\left[(\Delta_{12}\phi_{xz})^2 + (\Delta_{13}\phi_{xz})^2 + (\Delta_{23}\phi_{xz})^2 + (\Delta_{12}\phi_{xy})^2 + (\Delta_{13}\phi_{yz})^2 + (\Delta_{23}\phi_{yz})^2\right]\frac{T_c}{1+\omega^2 T_c^2} \quad (B.12)$$

and

$$P_2 = \frac{\pi^2 e^2 Q^2}{18h^2}\left\{\left[\Delta_{12}(\phi_{xx} - \phi_{yy})\right]^2 + \left[\Delta_{13}(\phi_{xx} - \phi_{yy})\right]^2 + \left[\Delta_{23}(\phi_{xx} - \phi_{yy})\right]^2 + 4\left[(\Delta_{12}\phi_{xy})^2 + (\Delta_{13}\phi_{xy})^2 + (\Delta_{23}\phi_{xy})^2\right]\right\}\frac{T_c}{1+\omega^2 T_c^2} \quad (B.13)$$

where $\Delta_{ab}\phi_{ij} = (\phi_{ij})_a - (\phi_{ij})_b$, a and b denoting site numbers.

These expressions for the $\Delta m = 1,2$ transition probabilities will now be used to calculate the relaxation times for the cases under consideration. The first of these is saturation of the two lines at a crossing point. The three levels are populated at equilibrium with N_{-1}, N_0 and

N_{+1} nuclei in the m = -1, m = 0 and m = +1 levels respectively. Because the levels are almost equally spaced, one can to good approximation let $N_0 - N_{-1} = n_0$ and $N_{+1} - N_0 = n_0$. Let n_1, n_2 and n_3 denote variations from equilibrium of the populations of levels m = -1,0 and +1 respectively. These populations then may be pictured as in Fig. 30, where $n_1 = -n_2-n_3$. The signal observed at time t is proportional to $2n_s$, where $n_s = n_3-n_2+n_0$.

$$\dot{n}_3 = -n_3P_1-n_3P_2+n_2P_1-(n_3+n_2)P_2$$

$$= -n_2(P_1+2P_2) + n_2(P_1-P_2) \qquad (B.14)$$

but $n_2 = 0$ and $\dot{n}_2 = 0$ so that $\dot{n}_3 + (P_1+2P_2)n_3 = 0$, which has the solution $n_3 = -n_0e^{-(P_1+2P_2)t}$, and by symmetry $n_1 = n_0e^{-(P_1+2P_2)t}$. Then $n_s = n_0-n_0e^{-(P_1+2P_2)t}$

$= n_0(1-e^{-t/T_1})$ where $1/T_1 = P_1+2P_2$ and thus $S_0-S_{(t)} = S_0e^{-t/T_1}$ where S_0 is equilibrium signal height.

Now for the case wherein only one of the lines is saturated, the populations are disturbed as pictured in Fig. 31. The signal at time t is proportional to n_s and $n_s = n_2-(-n_0+n_1)$.

$$\dot{n}_1 = -n_1(P_1+2P_2) + n_2(P_1-P_2) \qquad (B.15)$$

and $$\dot{n}_2 = -2P_1n_2 + P_1n_1 - P_1(n_2+n_1) = -3P_1n_2. \qquad (B.16)$$

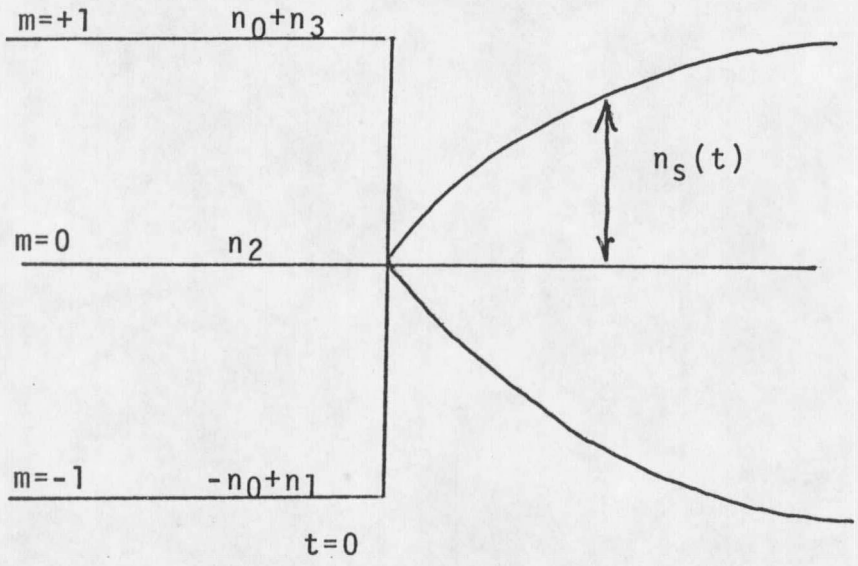


Fig. 31. Relative Populations of Nuclear Levels as a Function of Time for Symmetric Saturation. At t = 0, a 90° Pulse Saturates the System.

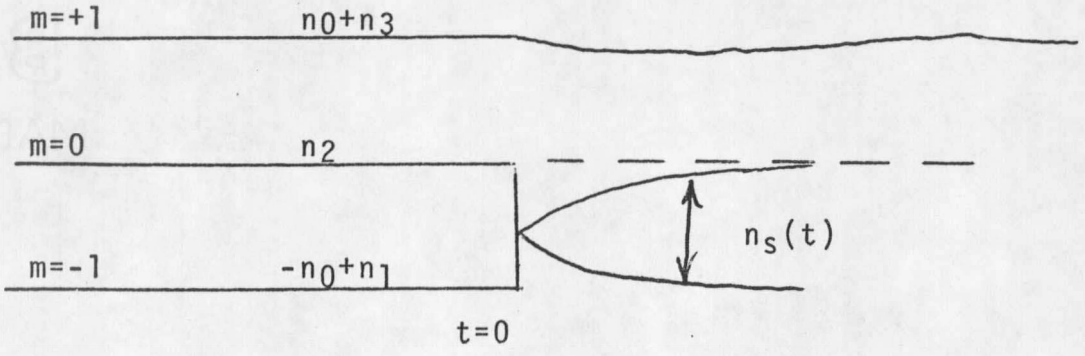


Fig. 32. Relative Populations of Nuclear Levels as a Function of Time for Saturation of Single Line. At t = 0 90° Pulse Saturates m = (0↔-1) Transition.

These equations are satisfied by $n_2 = \frac{-n_0 e^{-3P_1 t}}{2}$ and

$$n_1 = \frac{n_0 e^{-3P_1 t}}{4} + \frac{n_0 e^{-(P_1+2P_2)t}}{4}$$ making

$$n_s = n_0(1-\tfrac{3}{4}e^{-3P_1 t}-\tfrac{1}{4}e^{-(P_1+2P_2)t}) \text{ and}$$

$$S_0-S(t) = \tfrac{1}{4}(3e^{-3P_1 t} + e^{-(P_1+2P_2)t})S_0. \qquad (3.15)$$

Finally the mechanism proposed for relaxing the ND_3 deuterons by exchange to ND_2 sites is considered.

The population of the m = -1,0,+1 levels are denoted as pictured in Fig. 32. Since there are three ND_3 sites to every two ND_2 sites the populations are multiplied by the appropriate numerical factors. The experiment is carried out at a crossing, guaranteeing symmetric saturation of the ND_3 system. This makes $n_{32} = 0$ for all t, $n_{23} = -n_{21}$, and $n_{33} = -n_{31}$. Then the rate equation governing n_{31} is given by

$$\dot{n}_{31} = -p(n_{31}-n_{21}) \qquad (B.17)$$

where p denotes the probability that a deuteron at an ND_3 site jumps to an ND_2 site.

The rate equation for the corresponding level of deuterons of the ND_2 group is

$$\dot{n}_{21} = -(P_1+2P_2+\tfrac{3}{2}p)n_{21}+\tfrac{3}{2}pn_{31}. \qquad (B.18)$$

P_1+2P_2 is identified as $1/T_1$ governing relaxation for the case of symmetric saturation of the three level deuteron system and will be denoted P.

By substitution, the following differential equation for n_{31} is obtained

$$\ddot{n}_{31}+\frac{5}{2}p\dot{n}_{31}+P\dot{n}_{31}+Ppn_{31} = 0 \ . \qquad \text{(B.19)}$$

No confusion will be encountered by dropping the subscript 1 since the ND_3 as well as the ND_2 rates are symmetric in levels 1 and 3.

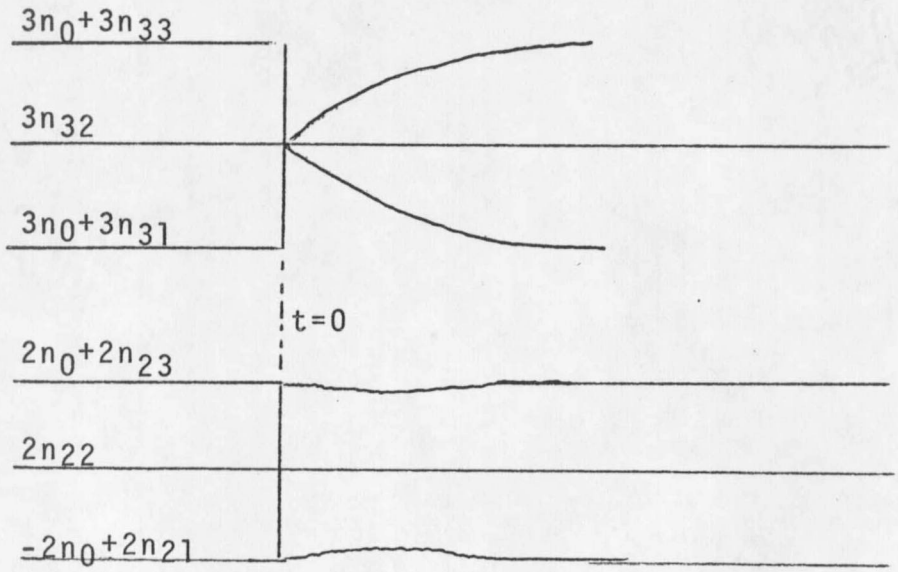


Fig. 33. Relative Populations of Nuclear Levels as a Function of Time for Symmetric Saturation of the ND_3 System, Indicating Coupling with ND_2 System.

Assuming the solution $n_3 = n_a e^{c_1 t} + n_b e^{c_2 t}$, with $n_a + n_b = n_0$, and that $P >> p$,* a solution $n_3 = n_a e^{-Pt} + n_b e^{-pt}$ is obtained.

Now since $P >> p$, i.e., the jumping between ND_3 and ND_2 sites occurs much more slowly than the relaxation of deuterons of the ND_2 group, the relaxation rate is limited by p, because $n_a \simeq 0$ and $n_b \simeq n_0$, with the result that $n_3 \simeq n_0 e^{-pt}$.

If the ND_2 system is saturated, the relaxation is due primarily to jumping between the two ND_2 sites. Since $n_{13} = 0$ it follows from Eq. (B.18) that the time constant for the return to equilibrium is $(P_1 + 2P_2) + \frac{3}{2}p$. However, the experiment for the ND_2 group is not carried out at a crossing, so the T_1 due to ND_2 hindered rotation is governed by Eq. (3.15), rather than $(P_1 + 2P_2)$, plus the correction $\frac{3}{2}p$ due to jumping between ND_2 and ND_3 sites.

---

*The latter assumption is justified since the basis of the proposed mechanism is the experimental observation that deuterons of the ND_2 group relax via P_1 and P_2 much faster than the deuterons of the ND_3 group relax.

APPENDIX C

Table XI and Fig. 34 summarize the recently available structural information[41] on $LiN_2D_5SO_4$. The N-D distances indicated in Table XI are not in good agreement with the N-H distances included in Table III. However, the general features of the structure are much the same.

TABLE XI

Bonded Distances

Bond	Distance	Bond	Distance
S -O(1)	1.484	N(1)-D(1)	1.018
S -O(2)	1.487	N(1)-D(2)	1.030
S -O(3)	1.467	N(2)-D(3)	1.015
S -O(4)	1.476	N(2)-D(4)	1.022
N(1)-N(2)	1.425	N(2)-D(5)	1.024

Non-Bonded Distances

Li-O(1)'	1.942	D(2)-N(1)'	2.042
Li-O(2)"	1.993	D(3)-O(1)	1.907
Li-O(3)	1.949	D(4)-O(2)	1.932
Li-O(4)	1.922	D(5)-O(2)	2.064

' and " = related by symmetry operation

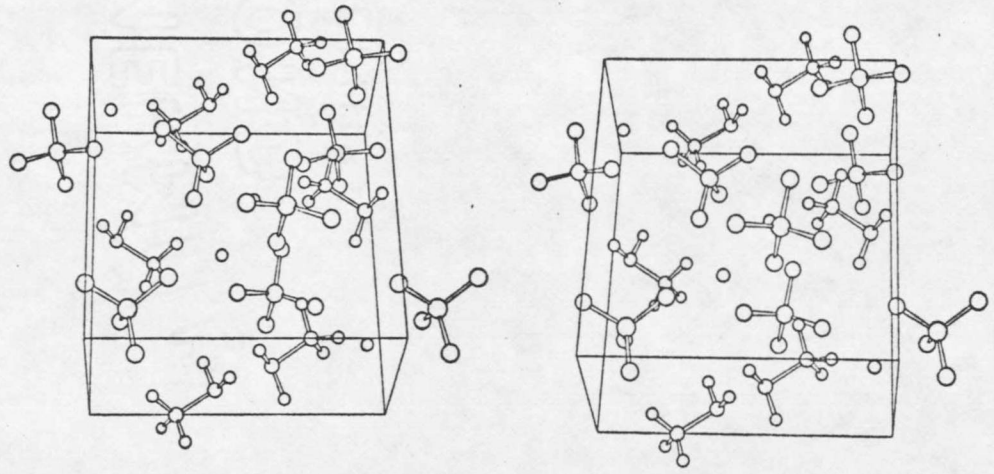


Fig. 34. Stereoscopic View of a Unit Cell of $LiN_2D_5SO_4$. View Is Down c Axis with Positive a Axis to Right of Viewer. (After Ross and Hamilton(40))

LITERATURE CITED

1. F. Jona and G. Shirane, Ferroelectric Crystals, The MacMillan Co., New York, 1962.

2. V. H. Schmidt, PhD Thesis, University of Washington (1961).

3. J. L. Bjorkstam and E. A. Uehling, Phys. Rev. 114, 961 (1959).

4. V. H. Schmidt and E. A. Uehling, Phys. Rev. 126, 447 (1962).

5. H. B. Silsbee, E. A. Uehling, and V. H. Schmidt, Phys. Rev. 133, A165 (1964).

6. J. L. Bjorkstam, Phys. Rev. 153, 599 (1967).

7. V. H. Schmidt, Phys. Rev. 164, 749 (1967); ibid. 173, 630 (1968).

8. A. Abragam, The Principles of Nuclear Magnetism, Oxford University Press, London, 1961.

9. C. P. Schlicter, Principles of Magnetic Resonance, Harper and Row, New York, 1963.

10. R. Pepinsky, K. Vedam, Y. Okaya, and S. Hoshino, Phys. Rev. 111, 1467 (1958).

11. V. M. Padmanabhan and R. Balasubramanian, Act. Cryst. 22, 532 (1967).

12. J. D. Cuthbert and H. E. Petch, Can. J. Phys. 41, 1629 (1963).

13. W. D. MacClement, M. Pintar, and H. E. Petch, Can. J. Phys. 45, 3257 (1967).

14. N. Niizeki and H. Koizumi, J. Phys. Soc. Japan 19, 132 (1964).

15. I. D. Brown, Acta. Cryst. 17, 654 (1964).

16. J. H. Van den Hende and H. Boutin, Acta. Cryst. 17, 660 (1964).

17. T. . Chiba, J. Chem. Phys. 41, 1352 (1964).

18. R. Blinc and D. Hadzi, Nature 212, 1307 (1966).

19. T. Chiba, Bull. Chem. Soc. Japan 38, 259 (1965).

20. R. Vijaraghaban and V. Saraswati, J. Phys. Soc. Japan 20, 2290 (1965).

21. W. Derbyshire, T. Gorvin and D. Warner, Molecular Phys. 12, 299 (1967).

22. T. Chiba, Bull. Chem. Soc. Japan 38, 490 (1965).

23. M. Linzer and R. Foreman, J. Chem. Phys. 46, 4690 (1967).

24. S. Rabideau and P. Waldstein, J. Chem. Phys. 45, 4600 (1966).

25. D. O'Reilly and T. Tsang, J. Chem. Phys. 46, 1291 (1967).

26. W. C. Hamilton and Ibers, Hydrogen Bonding in Solids, W. A. Benjamin Co. Inc., New York, 1968, pp. 260-265.

27. A. V. R. Warrier and P. S. Narayanan, Proc. Indian Acad. Sci. 64A, 254 (1966).

28. R. S. Krishnan and K. Krishnan, Proc. Indian Acad. Sci. 61A, 122 (1965).

29. J. Vanderkooy, J. Cuthbert, and H. E. Petch, Can. J. Phys. 42, 1871 (1964).

30. S. Devanarayanan and K. R. K. Easwaran, Proc. Indian Acad. Sci. 64A, 173 (1966).

31. T. Chiba, J. Chem. Phys. 39, 947 (1963).

32. F. N. H. Robinson, J. Sci. Instr. 36, 481 (1959).

33. F. J. Blankenburg, R. R. Knispel, and V. H. Schmidt, Rev. Sci. Inst. 37, 1020 (1966).

34. R. Knispel, PhD Thesis, Montana State University (1969).

35. W. G. Clark, Rev. Sci. Inst. 35, 316 (1963).

36. W. G. Clark and A. L. Kerlin, Rev. Sci. Inst. 38, 1593 (1967).

37. T. P. Das and E. L. Hahn, Nuclear Quadrupole Resonance Spectroscopy, Academic Press Inc., New York, 1958.

38. M. H. Cohen and F. Reif, Solid State Physics, Academic Press Inc., New York, 1957, Vol. 5.

39. G. M. Volkoff, Can. J. Phys. 31, 820 (1953).

40. G. M. Volkoff, H. E. Petch, and D. W. L. Smellie, Can. J. Phys. 30, 270 (1952).

41. F. Ross and W. Hamilton (private communication)

MONTANA STATE UNIVERSITY LIBRARIES
3 1762 10005644 7

D378
H839
cop.2

Howell, Francis L.
Hydrogen bonding in lithium hydrazinium sulfate

NAME AND ADDRESS
PENG CHENG LIN
1011 S. Tracy (G) PT
R J
D378
H839
Cop. 2